Geophys. J. Int. (2004) **156,** 506–526 doi: 10.1111/j.1365-246X.2004.02092.x

A reappraisal of earthquake focal mechanisms and active shortening in the Zagros mountains of Iran

Morteza Talebian and James Jackson

University of Cambridge, Department of Earth Sciences, Bullard Laboratories, Madingley Road, Cambridge CB3 OEZ*, UK.*
E-mail: talebian@esc.cam.ac.uk, jackson@esc.cam.ac.uk

Accepted 2003 July 7. Received 2003 July 3; in original form 2002 September 25

SUMMARY

The Zagros mountains of SW Iran are one of the most seismically active intra-continental fold-and-thrust belts on Earth, and an important element in the active tectonics of the Middle East. Surface faulting associated with earthquakes is extremely rare, and so most information about the active faulting comes from earthquakes. We use long-period teleseismic *P* and *SH* body waves to determine the orientation and depth of faulting in 16 new earthquakes, and then evaluate and synthesize all the available teleseismic data on earthquake source parameters in the Zagros. We use this information to investigate the style and distribution of active faulting in the Zagros, and how it contributes to the N–S shortening of the Arabia–Eurasia collision. When the data are ranked in quality and carefully evaluated, simple patterns are seen that are not apparent when routine catalogue data are taken at face value. An important change in the fault configuration occurs along strike of the belt. In the NW, overall convergence is oblique to the trend of the belt and the surface anticlines, and is achieved by a spatial separation ('partitioning') of the orthogonal strike-slip and shortening components on separate parallel fault systems. By contrast, in the SE, overall convergence is orthogonal to the regional strike and achieved purely by thrusting. In the central Zagros, between these two structural regimes, deformation involves parallel strike-slip faults that rotate about vertical axes, allowing extension along the strike of the belt. The overall configuration is similar to that seen in other curved shortening belts, such as the Himalaya and the Java–Sumatra trench. All the Zagros earthquakes we have been able to check have centroids shallower than ∼20 km and are confined to the upper crust. Many of the larger earthquakes are likely to occur in the basement beneath the sedimentary cover, which is active even beneath areas of known shallow structural decollement such as the Dezful embayment. The dominant style of shortening is high-angle reverse faulting with dips $>30^\circ$ though some lower-angle thrusting occurs in places. Active thrust and reverse faulting is relatively confined to the lower topography on the SW edge of the belt today, and only strike-slip faulting affects the higher topography. Profound vertical changes in structural and stratigraphic level indicate that a similar style of deformation was once active across the width of the Simple Folded Belt, but has progressively migrated SW over the last 5 Ma. There is no evidence for a seismically active structural decollement, such as a low-angle thrust, beneath the Zagros, nor is there any seismic evidence for active subduction, either beneath the Zagros or beneath central Iran. Instead the Arabian margin seems to have shortened by distributed thickening of the basement. Only in the syntaxis of the Oman Line, at the SE end of the Zagros, is there any evidence for a low-angle thrust of regional extent. Here, earthquakes continue 50 km north of the Zagros Thrust Line (the geological suture between the Arabian margin and central Iran) reaching depths of ∼30 km, and may represent thrusting of Arabian basement beneath central Iran to this extent.

Key words: active tectonics, continental tectonics, earthquakes, faulting, Iran, seismology, Zagros.

1 INTRODUCTION

The Zagros mountains of SW Iran form a linear intra-continental fold-and-thrust belt trending NW–SE between the Arabian shield and central Iran (Fig. 1). It is one of the most seismically active belts in Asia today, with frequent earthquakes of up to M_s 7.0. With its high level of seismicity, together with its apparent structural simplicity and geological youth, the Zagros has been influential in studies of continental shortening. It is extremely rare for coseismic surface faulting to be associated with Zagros earthquakes, so the most accessible information relating to active faulting comes from earthquake seismology. At different times, the seismicity of the Zagros has therefore attracted attention, usually related to specific questions such as whether the earthquake depths show any evidence of intra-continental subduction, the interaction between basement faulting and shortening in the sedimentary cover, and whether the shortening is achieved by high-angle reverse faulting or low-angle thrusts.

In spite of these earlier studies, major questions remain, such as the significance of strike-slip faulting in the Zagros and its role in the Arabia–central Iran collision. Moreover, there is now considerable renewed interest in hydrocarbon exploration and production in this region, which contains some of the most prodigious resources in the Middle East. As geologists need to construct structural cross-sections at depth, an important constraint on their interpretations is the known distribution and orientation of the faulting revealed by earthquakes. The purpose of this paper is to assess and synthesize the teleseismic earthquake data that are available, and then to address the major question of how the Zagros accommodates the Arabia–Iran shortening.

Although focal mechanisms and locations are now automatically determined for moderate-sized earthquakes globally, and are available in various catalogues, such data on their own are insufficiently accurate for the tectonic and geological questions of interest here (as we will show), and can even be misleading. Much more reliable estimates of earthquake source parameters can be obtained by inversion of teleseismic body waves, a process that is now relatively routine, but time consuming. In this paper we present such analyses for 16 new earthquakes, increasing by 43 per cent the number that are now available. These high-quality mechanisms, together with a careful assessment of the other catalogue data, are now sufficiently abundant to reveal patterns that were previously hidden.

2 TECTONIC AND GEOLOGICAL BACKGROUND

2.1 Regional tectonics

At the longitude of central Iran, the overall Arabia–Eurasia convergence is roughly N–S at ~25–35 mm yr^{-1} (Figs 1 and 2). Uncertainty in this direction and rate exist because of ambiguities in the interpretation of sea-floor spreading data in the Red Sea and Gulf of Aden (De Mets *et al.* 1994; Jestin *et al.* 1994; Chu & Gordon 1998), or because of the poorly determined motion of Arabia with current GPS

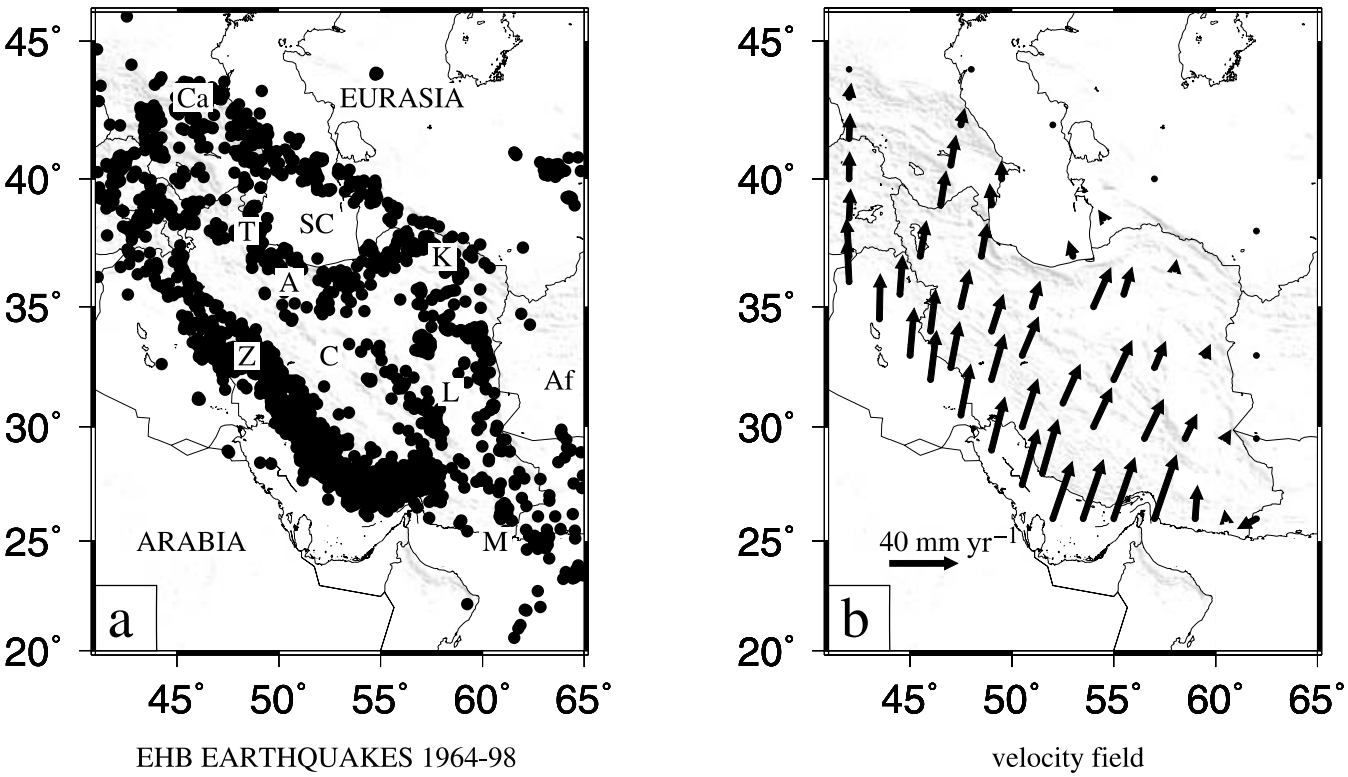

Figure 1. (a) Seismicity of Iran 1964–98, with epicentres from the catalogue of Engdahl *et al.* (1998). The Zagros is marked by Z, the Alborz by A, the Kopeh Dagh by K, the Talesh by T, the South Caspian Basin by SC, the Caucasus by Ca, Afghanistan by Af, the Makran by M, the relatively aseismic central Iran block by C, and the Lut block by L. (b) A velocity field showing how the northward motion of Arabia relative to Asia is absorbed in Iran. The distribution of velocities within Iran is estimated from the spatial variation in the style of strain rates indicated by earthquakes (from Jackson *et al.* 1995). The velocity of the Arabian margin (SW border of Iran) was based on the Arabia–Africa motion estimated by Jestin *et al.* (1994), and probably has too great an eastward component. Recent GPS-based estimates of Arabia–Eurasia motion are slower, and suggest a more N–S direction of convergence (Tatar 2001; Hessami 2002; Sella *et al.* 2002), closer in direction to that predicted by De Mets *et al.* (1994); see Fig. 2.

coverage (Sella *et al.* 2002). The latest global plate model based on GPS results by Sella *et al.* (2002) gives lower estimates of the overall Arabia–Eurasia motion than the earlier non-GPS models. Since the Arabia–Eurasia Euler pole lies in the Mediterranean region, the convergence rate increases with longitude, with values about 5–10 mm yr^{-1} higher in the east of Iran than in the west (Fig. 2). Shortening is thought to be concentrated in the three main active belts of the Zagros, Kopeh Dagh-Alborz-Talesh and the central Caspian Sea (Fig. 1), with large areas of central Iran, the Dasht-e-Lut and South Caspian basin being relatively flat, aseismic, and undeformed. Thus any shortening taken up north of the Zagros should also require N–S right-lateral strike-slip faulting between central Iran and western Afghanistan, which is effectively part of stable Eurasia. Various attempts have been made to estimate the relative importance of the different active belts in Iran (e.g. Jackson & McKenzie 1984; Jackson *et al.* 1995, 2002), but no direct measurements of deformation rates were available for these studies and it has been known for some time that much of the deformation within Iran occurs aseismically (North 1974; Jackson & McKenzie 1988), so that summation of earthquake moments does not provide a reliable guide. Nonetheless, the similarity between the observed earthquake focal mechanisms and the orientation and style of faulting seen at the surface suggests that the aseismic component of deformation in Iran is similar in style and orientation to that released seismically (Jackson *et al.* 1995). New data are also starting to emerge from GPS studies, and preliminary results suggest that shortening across the central Zagros is roughly N–S at a rate of 10–12 mm yr^{-1} (Tatar 2001; Tatar *et al.* 2002; Hessami 2002). If correct, they imply that the Zagros accounts for between a third and a half of the total Arabia–Eurasia convergence.

This paper is more concerned with the geometry of the deformation than with the rates, but it is important to note that the expected direction of shortening across the Zagros is roughly N–S, and thus oblique to the NW–SE strike of the belt over much of its length (Fig. 2). East of $\sim 52^{\circ}$E the NW–SE folds of the Zagros swing into a E–W orientation, and become roughly perpendicular to the overall shortening.

2.2 Geology

The Zagros forms a distinct tectono-stratigraphic unit in Iran (Falcon 1974; Ricou *et al.* 1977; Setudehnia 1978; Koop & Stoneley 1982; Sharland *et al.* 2001). For much of the Mesozoic it was a subsiding, probably rifted, margin to Arabia. Along the NE edge of the Zagros, an important geological boundary called the 'Zagros Thrust Line' (Fig. 2), the 'Zagros Suture' or the 'Main Zagros Reverse Fault' by various authors (e.g. Stöcklin 1974; Falcon 1974; Berberian 1995) approximately separates the former rocks of the Arabian continental margin to the SW from metamorphic and volcanic rocks of central Iran to the NE (e.g. Berberian & King 1981). This geological boundary is also an important seismotectonic feature today, marking an abrupt cutoff between the intense seismicity of the Zagros and the almost aseismic central Iran plateau (Fig. 1a).

The Zagros Thrust Line (and its equivalents) forms the NE border of the NW–SE trending High Zagros Thrust Belt (Falcon 1974; Berberian 1995), which has the highest topography and rainfall in the region (Fig. 2). Peaks reach heights of 4000 m and gorges reveal deeper exposures into the cores of thrusted anticlines (reaching lower Paleozoic levels) than elsewhere in the Zagros. Some shortening occurred in the High Zagros in the Late Cretaceous, at which time ophiolitic rocks and deep sea sediments were emplaced onto the Arabian margin (Stoneley 1976). But ophiolite emplacement preceded the final suturing of Arabia with Central Iran, which probably began in the Miocene (Stoneley 1981). Moreover, the main shortening of the Arabian margin in the Zagros, including all of the Simple Folded Belt SW of the High Zagros, began even later, in the Pliocene, probably only 3–5 Ma ago (Falcon 1974). This is also close to the time at which there is a major reorganization of the sedimentation and deformation in the South Caspian Basin (Devlin *et al.* 1999; Jackson *et al.* 2002). We suspect that this time represents the final closure of the minor oceanic and marginal basins that make up central Iran (Berberian & King 1981; McCall 1996) and the onset of true intra-continental shortening.

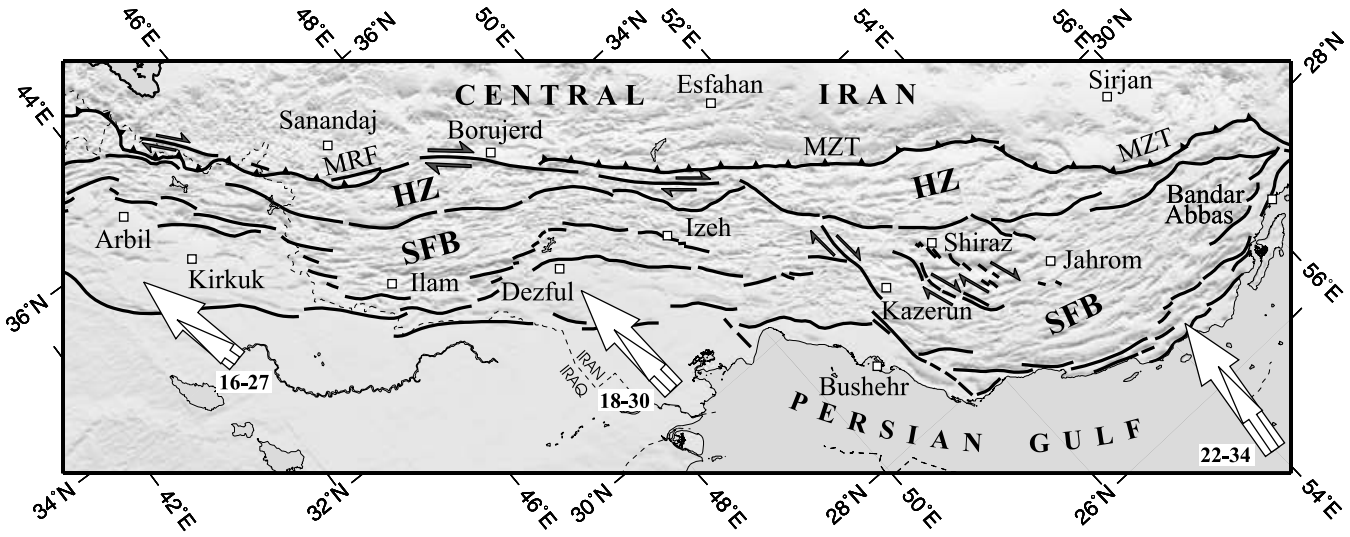

Figure 2. Location map, showing the main geographic regions discussed in the text. MRF is the Main Recent Fault, MZT is the Main Zagros Thrust, HZ is the High Zagros, SFB is the Simple Folded Belt. The white arrows show two estimates of the overall Arabia–Eurasia motion: the larger arrows are the estimates from De Mets *et al.* (1994) and the smaller arrows are the estimates from Sella *et al.* (2002). Numbers next to the arrows are the velocities corresponding to each of these estimates, in mm yr^{-1}. Solid lines are major inferred basement faults, from Berberian (1995).

Most of the larger earthquakes in the Zagros occur within the Simple Folded Belt (Fig. 2), characterized by large open anticlines with widths of typically 10 km and lengths of 100 km or more. Within the Simple Folded Belt exposures of stratigraphic levels deeper than the Jurassic are rare, probably because of numerous decoupling horizons of thick evaporitic sequences within the Cenozoic, Mesozoic and Paleozoic successions. The most famous of these horizons is the infracambrian Hormuz Salt Formation, which forms very large domes and plugs in the southern Zagros (e.g. Talbot 1998). Metamorphic continental basement is thought to lie beneath the Hormuz Salt Formation (Falcon 1974), and the total thickness of sediments above this basement has been estimated (from stratigraphic arguments and aeromagnetic surveys) to be as much as 10 km, or even more in places. As we will see, this in turn suggests that many of the large earthquakes in the Zagros occur in the basement beneath the sedimentary cover, and that it is the failure of coseismic ruptures to propagate through the weak decoupling horizons that accounts for the lack of surface faulting following earthquakes (e.g. Jackson & Fitch 1981). Most of the folds in the Simple Folded Belt are asymmetric, with steeper (or even overturned) SW limbs. At shallow levels, this indicates that many are underlain by thrusts or reverse faults that dip NE, but whether this is also true at deeper levels remains less clear.

Superficially, the Zagros looks like a 2-D structure, but closer inspection reveals important variations along strike. In the NW Zagros a major NW–SE right-lateral strike-slip fault system roughly follows the Zagros Thrust Line for almost 800 km, from ∼37°N to ∼32°N (Fig. 2). This fault system, called the Main Recent Fault (Tchalenko & Braud 1974), is a major element in the active tectonics of the Middle East, and has been responsible for several large earthquakes. Its role appears to be to separate ('partition') the overall N–S convergence in that part of the Zagros into orthogonal NE-SW shortening and NW–SE right-lateral strike-slip. Its total offset is probably about 50 km, and it may be moving as quickly as 10–17 mm yr^{-1} (Talebian & Jackson 2002). The Main Recent Fault appears to end near 32°N, where a zone of N–S right-lateral strike-slip faults between 51°E and 53°E occupies a region in which the fold axes change from NW–SE in the NW to E–W in the SE. The width of the folded belt is also variable along strike, reaching almost 200 km in the SE and near 34°N, but being constricted to narrower than 100 km at two embayments near Kirkuk and Dezful (Fig. 2). The earthquake data contain information about the nature and significance of these changes along strike, to which we return later.

2.3 Earthquakes

Early studies of the Zagros used the presence of earthquakes deeper than 50 km in the International Seismological Centre (ISC) or US Geological Survey (USGS) catalogues to postulate subduction of the continental Arabian shield beneath the Zagros (Nowroozi 1971; Haynes & McQuillan 1974; Bird *et al.* 1975), a view sometimes repeated more recently (e.g. Moores & Twiss 1995). However, neither local seismograph networks, nor the modelling of teleseismic body waves from the larger earthquakes have found any focal depths deeper than 15–20 km (e.g. Jackson & Fitch 1981; Ni & Barazangi 1986; Baker *et al.* 1993; Maggi *et al.* 2000a). Moreover, in an earlier study Jackson (1980a) showed that the apparently deep earthquakes were mostly poorly recorded by relatively few stations, which increases the trade-off between origin time and depth. Both the Harvard (Harvard 2002) and USGS (USGS 2002) Centroid Moment Tensor (CMT) catalogues have reported depths as great as 80 km, even for quite large earthquakes whose waveforms can be studied in detail. Maggi *et al.* (2000a) investigated three such earthquakes reported at depths of 40–80 km and showed that they were all shallow (10–15 km). They concluded that there was no evidence for any earthquakes deeper than about 20 km in the Zagros, and that view is not contradicted by the new data we present here. Thus there is no evidence, at least in the form of sub-crustal earthquakes, for continuing subduction of Arabia beneath Iran, and we will not return to that issue here, though there remain other interesting questions to ask about earthquake depths in the Zagros.

Most teleseismic determinations of focal mechanisms in the Zagros show reverse faulting with strikes parallel to those of the local fold axes. Jackson (1980b) observed that dips of nodal planes are typically in the range 30–60°, similar to that observed for active normal faults worldwide, and suggested that today's reverse faulting earthquakes were occurring on reactivated old normal faults inherited from the Paleozoic-Mesozoic extension of the Arabian margin. In the case of the Zagros, this reactivation mechanism remains speculation, though it has now been demonstrated elsewhere (e.g. Badley *et al.* 1989). This earlier work was based on focal mechanisms determined from first motion polarities, and we will re-examine the dip pattern with the better data. Strike-slip mechanisms are also seen, principally in the known regions of strike-slip faulting associated with the Main Recent Fault and the zone in the central Zagros between 51–53°E (Fig. 2). The Harvard CMT catalogue includes two earthquakes in the Simple Folded Belt of the Zagros with normal faulting mechanisms, one of them at 80 km depth. If correct, these would be extremely interesting, but Maggi *et al.* (2000a) showed that they are both almost certainly shallow reverse faulting earthquakes. We have removed both of them from our compilation. The message is clear: that uncritical use of the routinely published catalogue data can be seriously misleading. This is not to undervalue the Harvard CMT catalogue, which is surely one of the most valuable and useful data sets ever assembled in seismology, but to point out that if an earthquake is really important (because it stands out, with an unusual mechanism or depth), it is best to check it independently if you can.

Berberian (1995) pointed out that, within the folded and faulted Zagros sedimentary cover, there are lines along which very large changes in stratigraphic relief occur. He speculated that these might correspond to places where the basement itself was involved in deeper thrusting, and called these structures 'master blind thrusts'. His interpretation was supported, at least in some places, by concentrations of large modern or historical earthquakes along the lines of the inferred deep structures. If correct, his view is important, because it emphasizes the significance of a relatively small number of major basement faults, in contrast to the shortening in the sedimentary cover, which is more evenly distributed by folding. This is certainly a possibility, because of the ability of the various evaporitic decoupling horizons to separate the two. We cannot test his hypothesis with our data, partly because we know that the instrumental epicentres on which we must rely may be in error by up to 10–20 km (Ambraseys 1978; Berberian 1979). We nonetheless include the positions of Berberian's inferred major basement faults on our maps, partly as a guide to where the major changes in stratigraphic level are found.

3 DATA ANALYSIS AND PRESENTATION

The principal data of interest here are the focal mechanisms and centroid depths of teleseismically recorded earthquakes. We have most

Table 1. Earthquakes whose focal mechanisms are constrained by *P* and *SH* body wave modelling. Columns are: year, month, day, origin time (hr:min), latitude, longitude, M_w, strike, dip, rake (nodal plane 1), strike, dip, rake (nodal plane 2), slip vector azimuth chosen for Fig. 8 (blank if ignored), centroid depth (km), fault type (T = thrust, S = strike-slip, N = normal) followed by the figure number in which the mechanism is shown (the suffix i means inset), reference (BJP = Baker *et al.* 1993; B = Baker 1993; MJPB = Maggi *et al.* 2000a; A = Appendix of this paper; W = Walker 2003).

Date			Time	Lat.	Long.	M_w	s1	d1	r1	s2	d2	r2	sv	z	f	Ref
1968	6	23	09:16	29.75	51.26	5.5	136	45	88	319	45	92	46	9	T6	BJP
1972	4	10	02:06	28.41	52.79	6.7	322	40	98	132	50	83	52	10	T6	BJP
1974	12	2	09:05	28.09	55.86	5.2	65	65	80	268	27	110	335	7	T7	B
1976	4	22	17:03	28.69	52.12	5.7	312	52	80	148	39	103	58	7	T6	BJP
1977	4	6	13:36	31.96	50.67	5.9	228	48	36	112	64	132	318	6	S	B
1977	12	10	05:46	27.68	56.60	5.6	291	28	138	59	72	68	329	18	T7i	MJPB
1980	10	19	17:24	32.70	48.58	5.6	327	19	120	115	74	80	25	17	T5i	MJPB
1983	7	12	11:34	27.61	56.40	5.9	227	50	75	70	42	107	340	17	T7i	MJPB
1985	2	2	20:52	28.36	52.97	5.6	128	37	91	307	53	89	38	11	T6	MJPB
1985	8	7	15:43	27.86	53.04	5.4	290	56	88	114	34	93	24	17	T7	B
1986	7	12	07:54	29.91	51.56	5.5	4	73	−159	268	70	−18	358	7	S6i	BJP
1987	4	29	01:45	27.42	56.11	5.6	265	41	112	57	53	72	327	10	T7i	MJPB
1987	12	18	16:24	28.15	56.66	5.8	160	44	−145	43	67	−52		10	N7i	B
1988	8	11	16:00	29.95	51.57	5.5	3	69	−175	271	85	−21	1	7	S6i	BJP
1988	8	11	16:04	29.90	51.66	5.8	350	82	−166	258	76	−8	348	9	S6i	BJP
1988	12	6	13:20	29.89	51.63	5.6	357	74	−16	262	73	−17	352	10	S6i	BJP
1990	11	6	18:45	28.23	55.46	6.5	275	30	101	82	61	84	352	7	T7	MJPB
1991	5	22	16:29	27.38	55.77	5.4	118	72	93	288	18	80	28	13	T7	A1
1991	7	24	09:45	36.59	44.03	5.5	101	58	84	292	32	99	11	11	T5	A2
1991	11	4	01:50	30.69	50.25	5.8	135	80	78	6	16	140	45	5	T6	A3
1993	6	22	16:32	30.17	50.81	5.2	301	44	65	154	51	112	64	5	T6	MJPB
1993	7	9	10:29	28.39	55.33	5.1	115	22	107	277	69	83	7	16	T7	A4
1994	3	1	03:49	29.14	52.63	5.9	149	75	177	239	87	15	329	13	S6	A5
1994	6	20	09:09	29.05	52.66	5.8	255	74	−3	346	87	−164	345	9	S6	MJPB
1994	7	31	05:15	32.67	48.41	5.5	288	17	90	108	73	90	18	14	T5i	MJPB
1995	4	22	00:21	30.97	49.93	5.1	121	61	92	297	29	86	31	14	T6	A7
1996	5	24	06:35	27.85	53.57	5.0	109	43	81	301	47	98	19	6	T7	A8
1997	4	19	05:53	28.02	56.88	5.5	219	47	13	120	81	136		19	S7i	MJPB
1997	10	3	11:28	27.79	54.73	5.3	89	81	88	281	9	102	359	4	T7	Fig.3
1997	10	20	06:09	28.46	57.26	5.2	244	19	47	109	76	103	19	28	T7i	MJPB
1998	6	15	1:14	31.71	50.77	5.0	78	68	75	294	26	123	348	5	T6	A9
1998	8	1	23:38	27.74	56.51	5.1	95	38	86	280	52	93	5	9	T7i	A10
1998	10	4	0:42	33.32	47.26	5.2	111	37	92	288	53	88	21	9	T5	A11
1998	10	5	2:20	33.26	47.26	5.3	290	51	84	119	39	97	29	7	T5	A12
1998	11	13	13:01	27.76	53.62	5.4	104	63	73	318	32	120	14	7	T7	A13
1999	3	4	05:38	28.34	57.19	6.2	314	18	128	95	76	79	5	28	T7i	W
1999	5	6	23:00	29.50	51.88	6.1	49	77	−12	142	78	−167	319	7	S6	A14
2000	3	5	09:40	27.95	56.47	5.4	313	44	101	117	47	80	27	12	T7i	A15
2000	5	3	09:01	29.66	50.80	5.1	292	26	53	152	69	6	62	5	T6	A16

faith in source parameters that are determined through the inversion of teleseismic long-period *P* and *SH* body waves. There are now 37 earthquakes in the Zagros whose source parameters have been determined in this way (Table 1), 16 of them with new solutions presented in this paper. The other 21 solutions were obtained in previous studies by Baker (1993), Baker *et al.* (1993) and Maggi *et al.* (2000a). The method we used in all these studies involved taking the digital broad-band records from stations of the GDSN in the epicentral range 30–90° and convolving them with a filter that reproduces the bandwidth of the old WWSSN 15–100 long period instruments. We then used the MT5 version (Zwick *et al.* 1994) of McCaffrey & Abers's (1988) and McCaffrey *et al.*'s (1991) algorithm, which inverts the *P* and *SH* waveform data to obtain the strike, dip, rake, centroid depth, seismic moment and the source time function, which is parameterized by a series of isosceles triangle elements of half-duration τ s. We always constrained the source to be a double-couple. The method and approach we used are described in detail elsewhere (e.g. Nábělek 1984; McCaffrey & Nábělek 1987; Molnar & Lyon-Caen 1989; Taymaz *et al.* 1991) and are too routine to justify repetition here. The solutions for the new earthquakes are presented in the Appendix (available in the online version of the paper), with the exception of one example below, shown to illustrate the method and its application.

The example in Fig. 3 is an earthquake of moderate size (M_w5.3) on 1997 October 3 in the southern Zagros, where the fold axes strike E–W. The Harvard CMT solution indicates a steep nodal plane striking ENE–WSW, with movement on the shallow nodal plane in a sense of top-to-the-north. Our inversion, although it also shows a steep E–W nodal plane, does not confirm the Harvard solution, finding instead a sense of top-to-the-south movement on the shallow-dipping plane (Fig. 3), amounting to an interchanging of the *P* and *T* axes. Our inversion is able to produce a reasonable fit to the observed *P* and *SH* waveforms, which are abundant though, as usual in Iran, there are few stations to the south. Of particular interest is the comparison between our solution and that of the Harvard CMT catalogue. When the synthetic seismograms from the two solutions

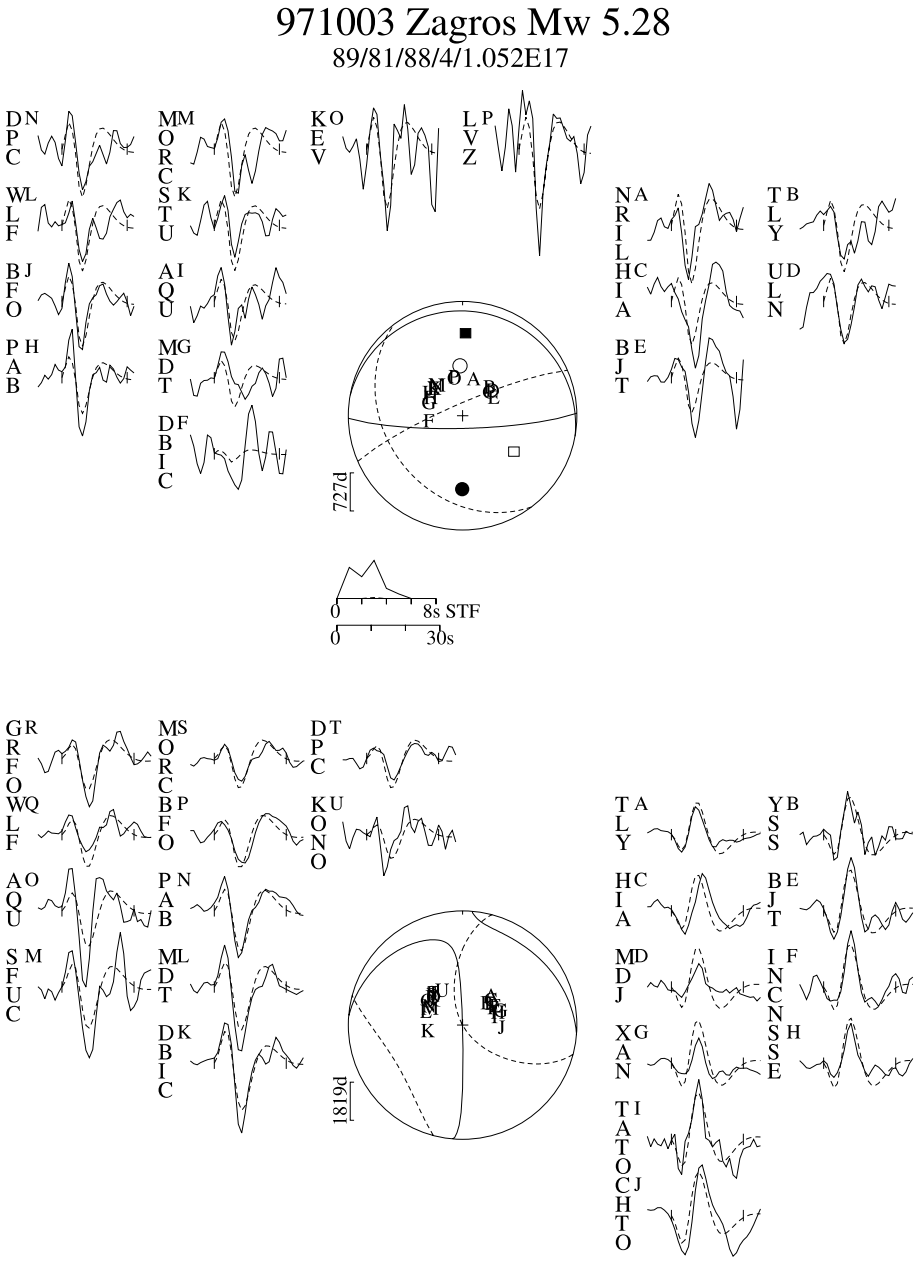

Figure 3. *P* (top) and *SH* (bottom) observed (solid) and synthetic (dashed) waveforms for an earthquake of M_w 5.3 in the Zagros on 1997 October 3 (Table 1). Station positions on focal spheres are identified by capital letters and arranged clockwise starting from north. STF is the source time function. Vertical ticks on the seismograms indicate the inversion window. Numbers beneath the header line are strike, dip, rake, centroid depth (km), and moment (Nm). Stations were weighted according to azimuthal density and then the S seismogram weights were halved, to compensate for their larger amplitudes. The solid lines on the focal spheres are the nodal planes for the solution and synthetic seismograms presented here. The black and white circles are the *P* and *T* axes respectively. The dashed nodal planes are for the Harvard CMT solution, with the black and white squares the corresponding *P* and *T* axes. Note that the CMT solution is not only different in orientation but also in polarity.

are compared with the observed (lines 1 and 2 in Fig. 4), it is clear that the Harvard solution cannot be correct as it has the incorrect first motion polarities for both *P* and *SH* waves. The problem cannot be in the onset times, because all our *P* wave alignments are fixed at the short period arrival times observed on broad-band records, and all our *SH* traveltime residuals are less than 4 s. This example illustrates, once again, the need to check unusual mechanisms in the Harvard catalogue.

To estimate uncertainties in source parameters we carried out tests in which one parameter was held fixed at values different from that in the final solution, while the other parameters remained free in the inversion. We then examined how far the value of the fixed parameter could be shifted before there was a substantial visual degradation in the fit between synthetic and observed seismograms. This methodology is illustrated in greater detail in Molnar & Lyon-Caen (1989) and Taymaz *et al.* (1991). An example is given in line 3 of Fig. 4, where we fixed the centroid depth to be 15 km, rather than the 4 km found in the inversion. The increased depth would naturally tend to broaden the first cycle of the waveforms, because of the greater time separation between the direct rays and the surface reflections, so the inversion tries to compensate by shortening the time function. Even so, it is unable to provide an acceptably narrow

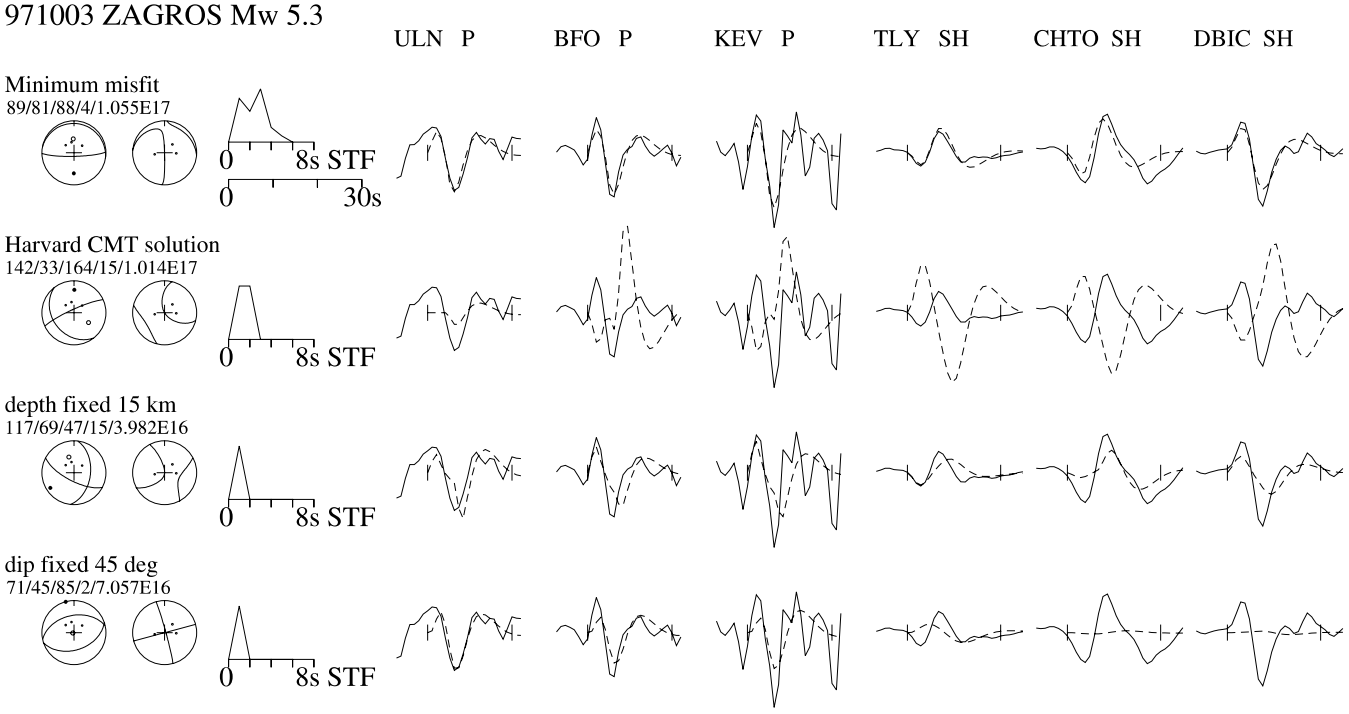

Figure 4. Tests to check the inversion for the 1997 October 3 earthquake (Fig. 3) for sensitivity to various source parameters (see text). Synthetic seismograms are dashed, observed are solid lines. The first line contains seismograms at selected stations from Fig. 3, the final inversion result. *P* and *SH* focal spheres are shown, with the time function and numbers showing the strike, dip, rake, depth and moment. In the second line the strike, dip, rake and depth were fixed to those of the Harvard CMT 'best-double-couple' solution, with all other parameters left free in the inversion. The fit to both *P* and *SH* waveforms is bad and, in particular, the first motion polarities of the synthetic seismograms are incorrect. In the third line the depth was fixed at 15 km, with other parameters free. The solution tries to compensate for the greater depth by shortening the duration of the time function, but is still unable to produce a short enough pulse, particularly for the *P* waves. In the fourth line the dip was fixed at 45°, with all other parameters free. With this dip, the solution is unable to match the *SH* waveforms.

pulse and the fit, particularly for *P* waves, is poorer. In line 4 of Fig. 4 we fixed the dip to 45°, a more usual value in the Zagros. The effect on the *P* waveforms is small, because all the stations lie in the compressional quadrant of the focal sphere anyway, but the inversion cannot match the *SH* waves, as *SH* positions become nodal along strike. The 45° dip is clearly incorrect. In this way we estimated the uncertainties to be approximately ±20° in strike, ±10° in dip, ±20° in rake and ±4 km in centroid depth. As usual for shallow earthquakes, there is some trade-off between depth and seismic moment, with shallower depths requiring higher moments to fit the observed seismograms (compare lines 1 and 3 in Fig. 4). We carried out the inversion in a half space with $V_p = 6.5$ km s^{-1} and $V_s = 3.7$ km s^{-1}. Realistic changes in the velocity model make little change to the source orientation or depth, but can affect the seismic moment. We estimate the uncertainty in moment to be ∼20 per cent.

Thus in this case we can conclude that the mechanism of the earthquake is unusual (because of the low dip to the north-dipping nodal plane and its relatively shallow depth), but not in the sense of the Harvard CMT solution. It may be significant that the correct focal mechanism contains a large M_{yz} component to the moment tensor, which is not well resolved by the Harvard CMT routine because the data is low-pass filtered (Dziewonski *et al.* 1981).

Where we were unable to analyse the waveforms ourselves (usually because they were too small) we make use of the Harvard CMT catalogue, which routinely publishes moment tensor analyses for earthquakes larger than about M_w 5.0. However, for shallow earthquakes the routine Harvard CMT solutions, again because of the low-pass filtering, do not accurately resolve the centroid depth, which is often fixed at an arbitrary 15 or 33 km. Moreover, because the CMT solution is not constrained to be a double-couple source, it often has an intermediate eigenvalue to the moment tensor that is significantly different from the zero value it would have if it were truly double-couple. This non-double-couple component may arise either from complications in the rupture process or from noise or other instabilities in the solution. In such cases the 'best-double-couple' solution (in which the intermediate eigenvalue is assigned a zero value and its corresponding eigenvector taken to be the B or null axis) may not be truly representative of the earthquake source as a whole. In our discussion we therefore separate those simple, well-determined CMT sources that appear to be good double-couples (i.e. more than 70 per cent double-couple component: see Table 2 for definition), from those that appear to have a greater non-double-couple component.

For some earthquakes that are too small for long-period waveform inversion and are earlier than the Harvard CMT catalogue, we have focal mechanisms based on long-period *P* wave first motions (Table 3). These have all been published before (McKenzie 1972; Jackson & McKenzie 1984) and all except two of them were read on instruments of the Worldwide Standard Seismograph Network (WWSSN) after 1963.

As far as depths are concerned, the best estimates are those from the complete inversions using both *P* and *SH* waves (Table 1), because the trade-off between source time function and depth is reduced. For 4 earthquakes, identified in Table 2, there were insufficient long-period *P* and *SH* waveforms for a complete source inversion, but enough to estimate the depth (one of these is new, and is reported in the Appendix). For some earlier (pre-GDSN) events

Table 2. Harvard CMT solutions for the Zagros. Columns are: year, month, day, origin time (hr:min), latitude, longitude, M_w, strike, dip, rake (nodal plane 1), strike, dip, rake (nodal plane 2), slip vector azimuth chosen for Fig. 8 (blank if ignored), centroid depth (km), percent double-couple, fault type (T = thrust, S = strike-slip) followed by the figure number in which the mechanism is shown, reference to independent depth estimates, if any (JF = Jackson & Fitch 1981; MJPB = Maggi *et al.* 2000a; NB = Ni & Barazangi 1986; A = Appendix of this paper), followed by a *P* if this depth estimate is based on *P* waves alone, by *S* if it is based on *SH* alone, or *P* + *SH* if both were used. If such an independent depth estimate is available, it is given in preference to the CMT depth. For the purposes of this paper, the percentage double-couple is expressed as a percentage (γ) according to the formula: $\gamma = 100\ \{1 - [(2|\lambda_2| \times 1.5)/(|\lambda_1| + |\lambda_3|)]\}$, where λ_1, λ_2 and λ_3 are the maximum, intermediate and minimum eigenvalues of moment tensor. In this (arbitrary) definition, $\gamma = 100$ per cent for a pure double-couple source (e.g. with eigenvalues $-1, 0, +1$) and 0 per cent for a linear vector dipole (e.g. with eigenvalues $-0.5, -0.5, +1.0$).

Date			Time	Lat.	Long.	M_w	s1	d1	r1	s2	d2	r2	sv	z	dc	f	Ref
1977	1	5	05:44	27.45	56.23	5.1	204	43	40	83	64	126	–	29	76	−7i	
1977	3	21	21:18	27.59	56.36	6.7	267	27	98	78	64	86	348	12	99	T7i	JF (P)
1977	3	21	22:42	27.61	56.47	6.1	241	26	78	75	65	96	345	19	78	T7i	
1977	3	22	11:57	27.60	56.42	5.9	75	43	96	247	47	85	345	12	76	T7i	MJPB (P+S)
1977	3	23	23:51	27.60	56.56	5.5	261	41	92	78	49	88	348	9	87	T7i	JF (P)
1977	4	1	13:36	27.56	56.29	5.9	262	44	90	82	46	90	352	12	79	T7i	JF (P)
1977	4	26	16:25	32.65	48.90	5.5	293	29	93	110	61	88	20	20	81	T5i	MJPB (P+S)
1977	6	5	04:45	32.61	48.07	6.1	293	34	91	111	56	89	21	12	76	T5i	JF (P)
1977	6	5	08:25	32.58	48.12	5.3	289	33	91	108	57	89	18	10	70	T5i	
1977	10	19	06:35	27.81	54.89	5.5	117	41	120	259	56	66	–	9	77	T7	NB (P)
1978	12	14	07:05	32.13	49.64	6.1	150	34	100	318	57	83	48	15	99	T6	
1979	3	28	01:33	30.88	49.94	5.2	317	42	92	135	48	89	45	15	93	T6	
1980	11	17	18:26	27.40	56.07	5.2	251	30	87	75	60	92	345	15	91	T7i	
1980	11	28	21:15	27.61	56.53	5.4	311	37	134	81	64	62	351	15	70	T7i	
1980	12	18	12:34	35.91	44.60	6.1	247	74	12	154	79	163	337	15	89	S5	
1981	1	2	04:57	32.73	48.47	5.3	277	24	95	92	66	88	2	15	80	T5i	
1981	4	1	10:16	29.82	51.48	5.2	351	34	144	111	71	61	–	15	89	−6i	
1981	4	16	10:27	27.72	56.35	5.1	221	42	8	125	85	132	–	15	70	S7i	
1983	2	7	15:06	26.86	57.57	5.9	5	42	172	101	85	48	–	33	100	S7	
1983	2	18	07:40	27.91	53.82	5.2	272	20	94	88	70	89	358	6	88	T7	MJPB (P)
1983	3	5	14:22	32.47	49.34	5.6	254	4	32	133	88	93	43	10	74	T5i	
1983	5	28	11:35	32.58	48.58	5.5	314	38	113	106	56	73	16	8	93	T5i	NB (P)
1984	12	22	16:05	27.82	54.45	5.1	115	41	84	303	49	95	25	49	97	T7	
1985	9	18	00:10	31.59	49.47	5.3	147	36	74	347	55	102	57	11	80	T6	
1986	5	2	03:18	28.00	53.31	5.5	107	47	57	331	52	121	17	15	64	T7	
1986	5	3	10:37	27.98	53.33	5.2	111	33	60	325	62	108	21	15	98	T7	
1986	12	20	23:47	29.90	51.58	5.4	348	70	−179	257	89	−20	347	15	59	S6i	
1987	5	29	06:27	34.07	48.27	5.3	218	80	2	128	88	170	308	15	28	S5	
1988	1	26	09:34	32.76	47.11	5.5	306	20	79	137	70	94	47	20	74	T5i	
1988	3	30	02:12	30.85	50.18	5.8	296	32	90	116	58	90	26	15	85	T6	
1988	6	9	00:09	28.28	56.87	5.2	310	11	139	81	83	82	351	15	59	T7i	
1988	8	30	17:30	29.96	51.72	5.1	242	57	−9	337	83	−147	332	16	64	S6i	MJPB (S)
1989	4	2	06:42	28.17	57.28	5.3	242	24	81	72	66	94	342	43	85	T7i	
1989	4	2	21:24	32.66	47.78	5.4	256	40	−7	351	85	−130	–	15	37	S5i	
1989	5	3	09:13	30.00	51.67	5.2	153	55	−166	55	78	−36	325	15	100	S6i	
1989	5	27	20:08	30.15	50.89	6.0	103	45	51	332	57	122	–	15	64	T6	
1990	8	3	11:57	32.80	48.21	5.3	96	33	53	318	64	111	48	15	96	T5i	
1990	10	11	13:56	32.86	48.20	5.0	128	45	90	308	45	90	38	15	100	T5i	
1990	12	16	22:18	29.00	51.31	5.7	332	23	97	144	67	87	54	15	74	T6	
1991	12	19	18:55	28.04	57.27	5.4	215	35	26	103	75	123	–	15	44	T7i	
1992	3	4	11:57	31.57	50.74	5.1	122	79	173	213	83	12	–	33	60	S6	
1992	9	11	12:06	29.92	51.12	5.3	302	33	67	148	60	104	58	15	71	T6	
1993	1	6	22:51	29.04	52.13	5.4	248	76	0	339	90	−166	338	15	47	S6	
1993	3	26	22:52	30.70	50.89	5.1	61	74	−3	152	88	−164	–	33	29	S6	
1993	3	29	15:20	28.01	52.74	5.2	104	28	72	305	64	99	35	13	85	T6	MJPB (P)
1993	4	12	14:00	28.23	57.13	4.9	292	44	97	103	46	84	13	33	100	T7i	
1993	10	21	21:52	30.19	51.23	5.0	105	41	101	271	50	80	15	15	99	T6	
1994	3	29	07:56	29.20	51.36	5.1	334	40	104	136	52	79	46	7	85	T6	A6 (P)
1994	3	30	19:55	28.98	52.79	5.4	148	71	177	239	87	19	329	33	77	S6	
1994	4	3	06:51	28.93	52.76	5.2	47	69	−11	142	79	−159	317	33	84	S6	
1994	9	20	05:51	32.53	48.73	5.2	103	25	87	286	65	91	16	15	93	T5i	
1995	1	24	04:14	27.59	55.67	4.9	217	31	56	75	64	109	345	15	26	T7	
1996	2	26	08:08	28.30	57.05	5.5	315	7	125	100	84	86	10	33	48	T7i	
1996	10	18	09:26	27.69	57.58	5.3	289	21	83	117	69	93	27	15	73	T7	
1996	11	18	11:52	29.94	51.56	5.2	177	62	−177	85	87	−28	355	33	75	S6i	

Table 2. (*Continued*).

Date			Time	Lat.	Long.	M_w	s1	d1	r1	s2	d2	r2	sv	z	dc	f	Ref
1997	5	5	15:11	27.07	53.89	5.0	296	52	128	64	52	52	–	15	11	T7	
1997	7	27	23:33	27.53	56.60	5.1	108	76	175	199	85	15	–	33	92	S7i	
1998	8	5	14:27	33.21	46.22	5.6	183	20	52	43	74	103	–	33	52	T5	
1998	8	21	05:13	34.31	48.19	4.9	25	39	−84	197	51	−95	287	9	82	N5	MJPB (P+S)
1998	9	21	21:35	31.08	51.25	5.1	78	71	12	343	78	160	348	33	88	S6	
1999	1	15	19:14	35.35	45.16	5.1	128	29	86	312	61	92	42	33	76	T5	
1999	4	30	4:20	27.84	53.54	5.1	321	53	134	82	55	47	–	45	86	T7	
1999	9	24	19:17	28.65	51.33	5.2	148	29	121	294	65	74	–	33	90	T6	
1999	10	31	15:09	29.41	51.81	5.2	117	34	67	324	58	105	54	33	99	T6	
2000	3	1	20:06	28.40	52.85	5.0	49	26	55	267	69	106	357	15	58	T6	
2000	6	23	06:15	30.16	51.65	5.1	180	75	175	272	85	15	2	33	78	S6i	
2000	9	13	13:09	27.82	51.68	4.9	126	26	144	249	75	68	–	44	66	−6	

Table 3. First motion fault plane solutions. Columns are: year, month, day, origin time (hr:min), latitude, longitude, M_w, strike, dip, rake (nodal plane 1), strike, dip, rake (nodal plane 2), slip vector azimuth chosen for Fig. 8 (blank if ignored), centroid depth from *P* wave modelling in km (if any), fault type (T = thrust, S = strike-slip) followed by the figure number in which the mechanism is shown, reference (M = McKenzie 1972; S=Shirakova 1967; NB = Ni & Barazangi 1986; KB = Kadinsky-Cade & Barazangi 1982; JM = Jackson & McKenzie 1984).

Date			Time	Lat.	Long.	M_w	s1	d1	r1	s2	d2	r2	sv	z	f	Ref
1957	12	13	1:45	34.55	47.80	6.7	6	52	125	137	50	54			T5	M
1958	8	16	19:13	34.30	48.17	6.6	325	70	170	58	81	20	328		S5	S
1963	3	24	12:44	34.43	48.00	5.8	314	52	−164	214	77	−39	304	8	S5	NB
1964	12	22	4:36	28.16	56.89	5.5	92	76	90	272	14	90	2	18	T7i	KB
1965	6	21	0:21	28.10	55.84	6.0	313	60	110	97	36	59		8	T7	NB
1966	7	27	14:49	32.67	48.78	5.3	294	34	119	80	61	72	350		T5i	M
1966	9	18	20:43	27.82	54.27	5.9	82	56	86	269	34	96	352	12	T7	NB
1967	1	11	11:20	34.07	45.66	5.6	140	50	81	334	41	101	50	10	T5	NB
1968	9	14	13:48	28.34	53.18	5.8	108	60	90	288	30	90	18	7	T7	NB
1970	2	23	11:22	27.82	54.47	5.6	106	46	90	286	44	90	16	9	T7	NB
1970	2	28	19:58	27.83	56.31	5.5	84	50	90	264	40	90	354		T7i	JM
1970	10	25	11:22	36.75	45.19	5.5	319	50	−154	212	70	−43	302		S5	JM
1971	4	12	19:03	28.26	55.61	5.9	81	55	90	261	35	90	351	10	T7	NB
1971	11	8	3:06	27.01	54.46	5.9	120	48	90	300	42	90	30	9	T7	NB
1971	12	9	1:42	27.29	56.37	5.8	276	40	55	138	58	116			T7i	JM
1972	6	12	13:34	33.04	46.27	5.0	114	56	83	306	35	100	24	11	T5	NB
1972	6	14	4:34	33.04	46.11	5.3	198	40	51	65	60	118			T5	JM
1972	7	2	12:56	30.06	50.85	5.3	132	64	90	312	26	90	42	9	T6	NB
1973	11	11	7:14	30.54	52.95	5.5	331	89	90	151	1	90			T6	JM
1975	3	7	7:04	27.48	56.23	6.1	90	60	90	270	30	90	0	11	T7i	KB
1975	12	24	11:48	27.02	55.48	5.5	80	56	90	260	34	90	350	8	T7	NB
1976	3	16	7:28	27.31	54.98	5.2	73	50	90	253	40	90	343	9	T7	NB
1976	11	7	11:08	33.21	47.90	4.8	138	58	121	269	43	50			T5	JM
1977	3	24	4:42	27.66	56.60	5.3	122	60	90	302	30	90	32		T7i	JM
1978	2	11	21:40	28.19	55.38	4.6	96	40	90	276	50	90	6		T7	JM

that we have not re-analysed, we have depth estimates based on long-period *P* waves alone, from earlier studies by Jackson & Fitch (1981), Kadinsky-Cade & Barazangi (1982) and Ni & Barazangi (1986). Since these are all determined from long-period waveforms, they are centroid depths, nominally at the centre of the fault plane. As a rough guide, an earthquake of M_w 6.0 is expected to have a fault area of $\sim 10 \times 10$ km^2, whereas one of M_w5.5 will have a fault area of $\sim 5 \times 5$ km^2.

Finally, we use, where possible, epicentres from the catalogue of Engdahl *et al.* (1998) and its updates, as these are likely to be better than those of the ISC and USGS. Thus our data for both focal mechanisms and centroid depths are arranged in a hierarchy, with each earthquake included only once in our compilation. For the focal mechanisms the hierarchy is, first, those based on body waveform analysis, then the CMT solutions with $M_w \geq 5.3$ and more than 70 per cent double-couple component, then other CMT solutions, and finally first motion solutions. For centroid depths the hierarchy is, first, those based on *P* and *SH* waveforms, then those based on *P* waveforms alone. Thus the reader can see all the solutions and depths that are available with some idea of quality. We have removed the two normal faulting CMT solutions that Maggi *et al.* (2000a) identified as incorrect.

4 RESULTS

4.1 Fault plane solutions

Our final compilation of focal mechanisms is shown in Figs 5–7, which together cover the whole Zagros and allow all the available data to be seen, as well as allow the origin of each solution to be identified. The general pattern of mechanisms is quite simple.

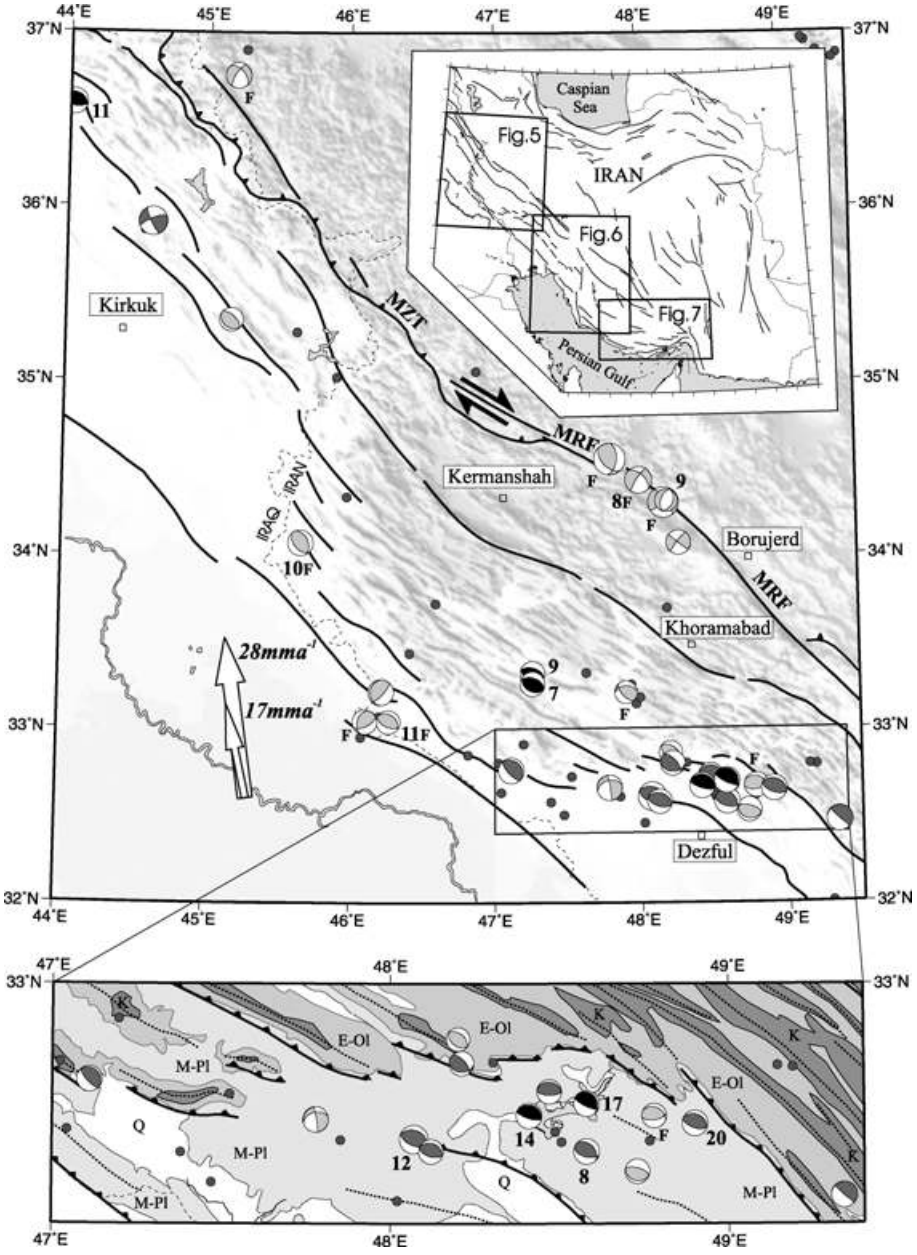

Figure 5. Summary of fault plane solutions in the NW Zagros (see inset top right for location). Each earthquake appears only once, with the solutions chosen in the following hierarchy. Focal spheres in black are those constrained by long-period *P* and *SH* body wave modelling (as in Fig. 3), and are listed in Table 1. Dark gray spheres are Harvard CMT solutions for earthquakes with $M_w \geq 5.3$ and with at least 70 per cent double-couple component. Light gray focal spheres are CMT solutions for other earthquakes ($M_w < 5.3$ or <70 per cent double-couple component) or first-motion solutions (marked by F). Where available, centroid depths in km, determined from waveform modelling, are marked alongside. All CMT solutions are listed in Table 2, and first-motion solutions are in Table 3. White arrows are the directions and rates of the overall Arabia–Eurasia motion from De Mets *et al.* (1994, big arrow) and Sella *et al.* (2002, small arrow). MZT is the Main Zagros Thrust, which is essentially the geological suture between rocks of the Arabian margin and central Iran. MRF is the right-lateral Main Recent Fault. Solid lines are probable major basement faults, identified by Berberian (1995) from substantial changes in stratigraphic level at the surface. Solid circles are other earthquakes of $m_b > 5$ from the catalogue of Engdahl *et al.* (1998). The inset at the bottom shows an enlargement of the Dezful embayment. The earthquakes are the same as in the main figure. The inset shows a summary of the geology: K is Cretaceous, E-Ol is Eocene-Oligocene, M-Pl is Miocene-Pliocene, Q is Quaternary. Dotted lines are anticline axes. Solid lines with triangles are the inferred positions of major thrusts at depth. The thrusts separating E-Ol from M-Pl follow the Main Mountain Front of Berberian (1995).

Only two normal faulting earthquakes are seen. A small event (M_w 4.9), but with an apparently reasonable (82 per cent double-couple) CMT solution occurred on 1998 August 21 near the Main Recent Fault (Fig. 5). This is in a region where the Main Recent Fault is known to have an extensional component of motion and is associated with a pull-apart geometry (Talebian & Jackson 2002). The second normal-faulting event (M_w 5.8) occurred on 1987 December 18 on the syntaxis associated with the Oman Line (Fig. 7 and inset b), showing E–W extension at a depth of 10 km. This is again a special place, above a deeper, low-angle thrust (discussed later), and indicates some extension perpendicular to the northward indentation of the Oman peninsular into Iran.

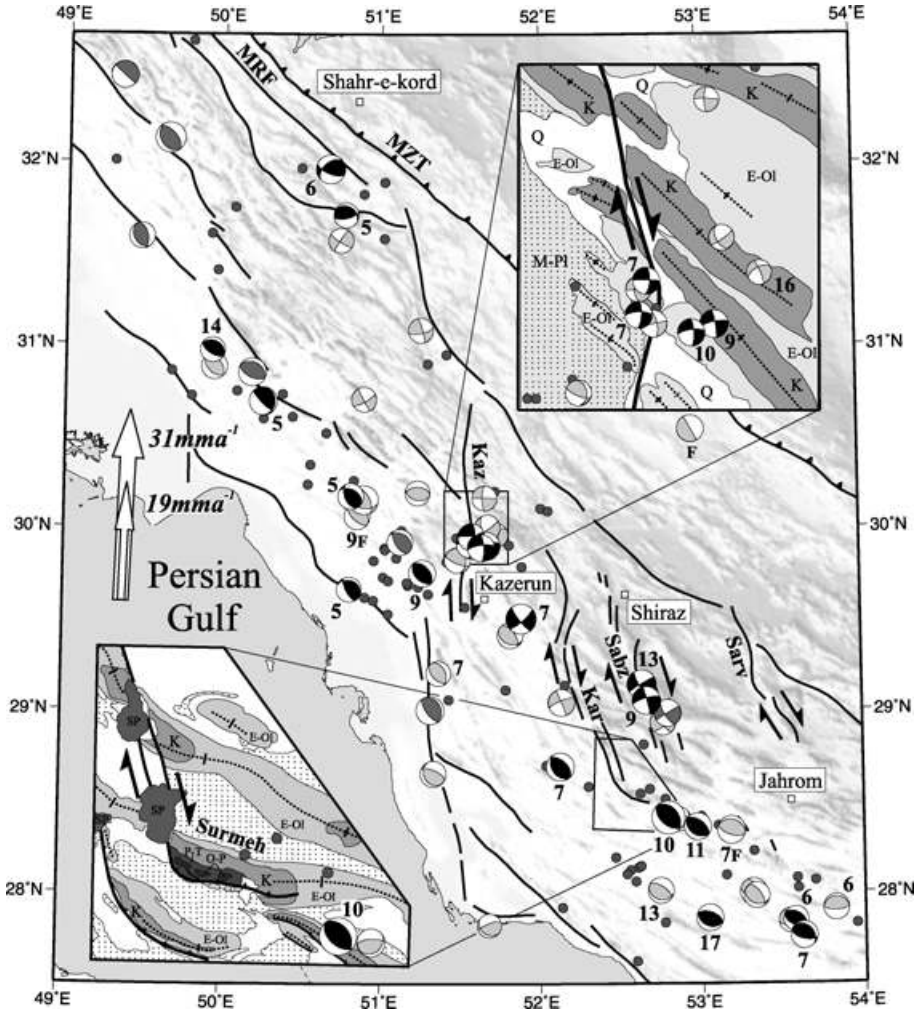

Figure 6. Summary of fault plane solutions in the central Zagros (see inset to Fig. 5 for location). Notation for earthquakes, faults and white arrows is the same as in Fig. 5. The main right-lateral strike-slip faults of the central Zagros are the Kazerun (Kaz), Karebas (Kar), Sabz Pushan (Sabz) and Sarvestan (Sarv) faults. The insets shows details near the Kazerun Fault and Kuh-e-Surmeh, with notation the same as in the inset to Fig. 5. SP are salt plugs of the Hormuz Salt Formation, O-P is Ordovician to Permian, and P-T is Permo-Triassic.

Strike-slip solutions are mostly associated with the NW–SE right-lateral Main Recent Fault system (Fig. 5) or with the roughly N–S right-lateral fault system in the central Zagros between 51–53°E (Fig. 6). Not all the epicentres of these events lie precisely on the known fault traces, but given the possible location error of up to 20 km, this may not be significant. There are a few scattered strike-slip solutions that are not associated with these known fault systems, but they are relatively rare.

Most of the focal mechanisms show reverse faulting, with strikes subparallel to the local trend of the topography and fold axes. Again, there are a few exceptions, but they are relatively rare. Near 33°N 46°E (Fig. 5) are two solutions with strikes nearly perpendicular to the fold axes. These occur at a prominent step in the Zagros range front (see e.g. Berberian 1995), and may be analogous to the faulting that is seen in relay steps in extensional fault systems, where the change in elevation along strike requires deformation with a dip-slip component (in this case shortening) orthogonal to the main structures. Such transverse faulting in relays is more significant as a source of fracturing in oil reservoirs at depth than as an indicator of regional tectonic patterns. Also remarkable is how nearly all the reverse and thrust faulting mechanisms show nearly pure dip-slip motion, with oblique slip being relatively rare. We discuss patterns in the dips and depths of these events later.

The only earthquake in the Zagros that is known to have produced unambiguous reverse-faulting coseismic surface ruptures is that of 1990 November 6 at Darab (28.2°N 55.5°E, Fig. 7). This event produced 15 km of scarps, with the north side up and an average vertical motion of ∼1.0 m (Raisi 1991). These field observations are compatible with the observed moment (7.1×10^{18} N m; M_w 6.5) and centroid depth (7 ± 4 km) for this event (Table 1): with a typical displacement-to-length ratio of 5×10^{-5} (Scholz 1982), we would expect a fault area of $\sim 17 \times 17$ km^2 and an average slip of ∼0.8 m. This unusual occurrence of surface ruptures may, in this case, be related to the epicentral location in the High Zagros, near the edge of the known distribution of the Hormuz Salt Formation.

Some, but not all, the reverse fault mechanisms are associated with the major (inferred) basement faults of Berberian (1995), which are shown as the thick lines in Figs 5–7. Particularly notable is the group of earthquakes west of Jahrom at ∼28.5°N 53°E, on a fold-parallel trend in the region of the 2000 m-high Kuh-e-Surmeh (Fig. 6, SW inset), which is one of the few areas in the Simple Folded Belt where lower Paleozoic rocks are brought to the surface, and where

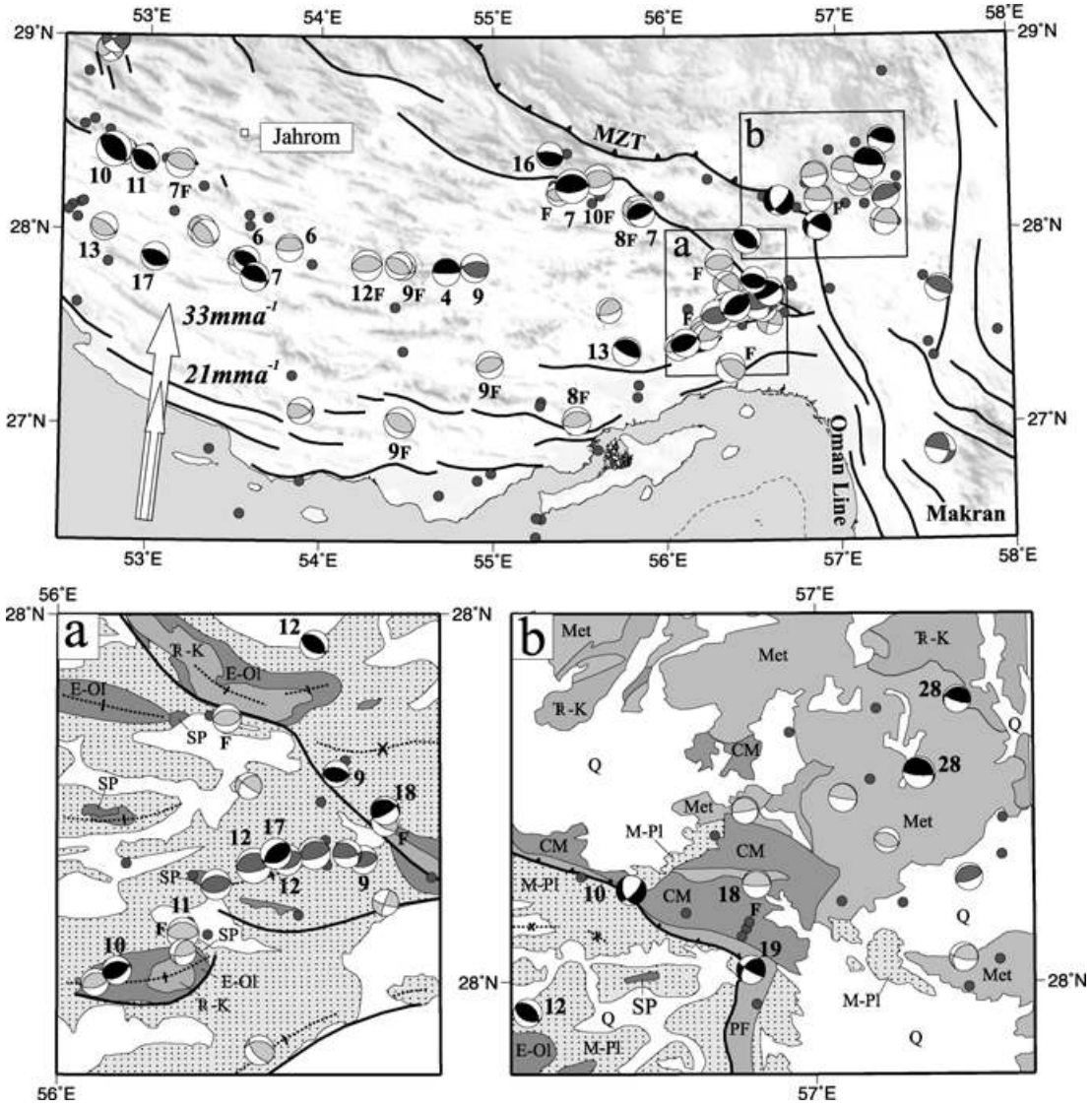

Figure 7. Summary of fault plane solutions in the SE Zagros (see inset to Fig. 5 for location). Notation is the same as in Figs 5 and 6. Two insets (a and b) are included to show details in the region of the Oman Line syntaxis. TR-K is Triassic-Cretaceous, CM is Cretaceous coloured melange, PF is Paleogene flysch, Met are undifferentiated metamorphic and igneous rocks. Other symbols are the same as in Fig. 5.

Berberian (1995) inferred a deep basement thrust. The highest elevations and deepest stratigraphic exposure occur where this basement thrust meets the southern end of the Karebas strike-slip fault. The Karebas fault thus seems to terminate in a thrust that dies away with distance from the junction, a geometry familiar elsewhere, and probably characteristic of strike-slip faults that rotate about a vertical axis (Bayasgalan *et al.* 1999). Other prominent lineations of reverse faulting earthquakes, such as those at ∼27.8°N 54.5°E and ∼27.5°N 56.5°E (both on Fig. 7) are also discussed further by Berberian (1995).

A region of particular interest is the Dezful embayment (Fig. 5, inset), not least because it is the main region of oil production in Iran. A substantial change in stratigraphic level occurs here, where the Eocene-Oligocene rocks (including the Asmari Limestone reservoir formation) that are exposed at the surface to the N and E sharply plunge to depths of 4–5 km along a line known as the Main Mountain Front, marked as a thrust in the inset to Fig. 5. This front is assumed to be the surface expression of a deep basement fault (Berberian 1995), yet the epicentres of several substantial earthquakes lie *south* of the front and within the Dezful embayment itself, i.e. in the *footwall* of the presumed frontal basement thrust. If these earthquakes were actually on that frontal fault their epicentres would have to lie nearly 40 km further north, and we do not believe they are all mislocated systematically by that amount. Moreover, some of these earthquakes in the embayment are the deepest that we have been able to confirm with waveform modelling, reaching depths of 20 km. This in turn suggests that the depression of the Tertiary stratigraphy is matched by lower levels of the basement as well. Within the embayment itself exposure is limited to rocks of Miocene and younger age, and it is often assumed that structures are all very superficial, restricted to levels above Mesozoic and Tertiary decoupling horizons. Yet the earthquake data strongly suggest that, at least in places, the Dezful embayment is underlain by major active basement faults as well.

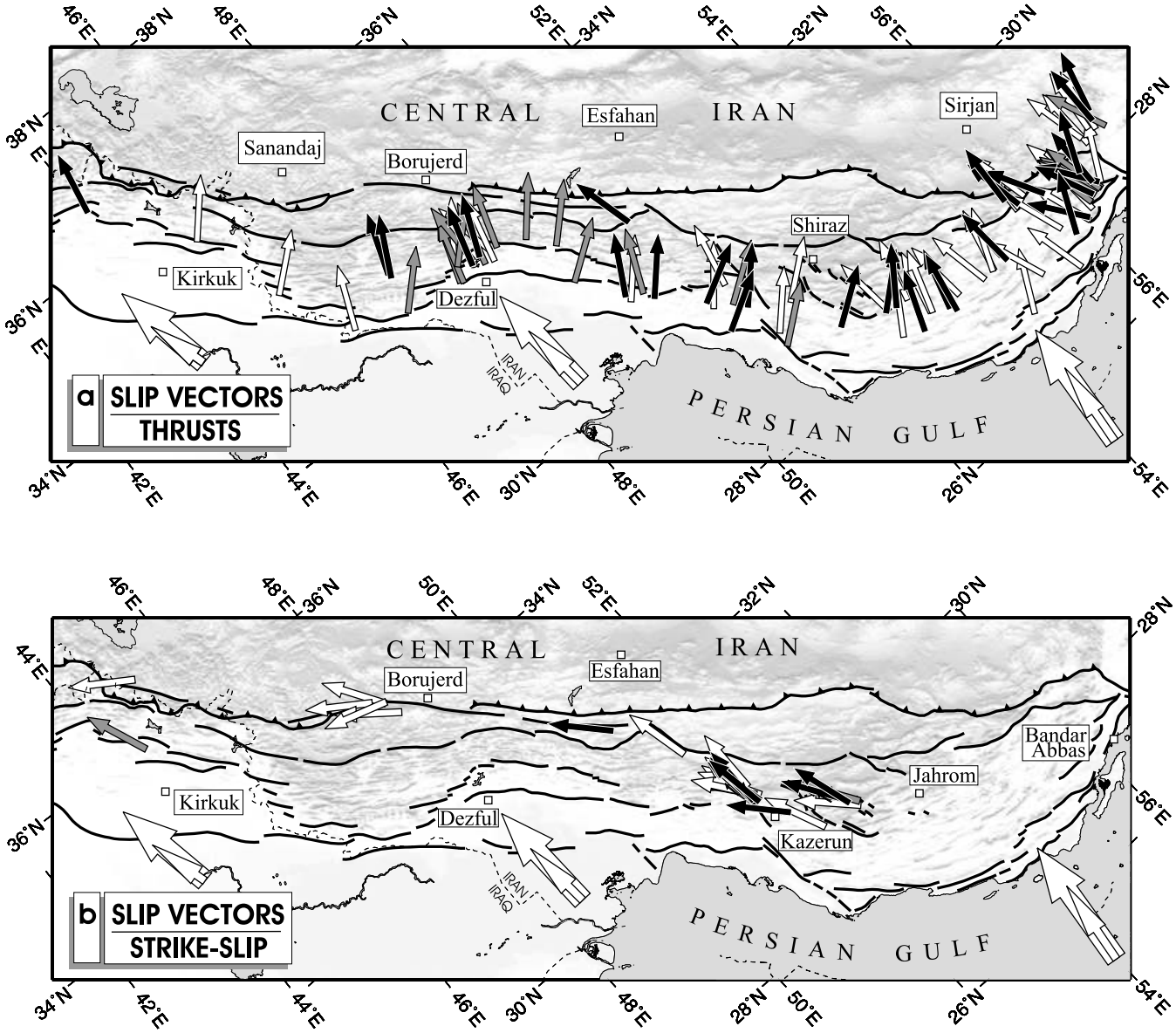

Figure 8. Earthquake slip vectors in the Zagros, showing the motion of the south or west side relative to the north or east (see text). Black, gray and small white arrows correspond to the focal mechanisms in black, dark gray and light gray in Figs 5, 6 and 7. Large white arrows are the estimated overall Arabia–Eurasia motions from De Mets *et al.* (1994) and Sella *et al.* (2002), as before. (a) Slip vectors from thrust or reverse faults. (b) Slip vectors from strike-slip faults.

4.2 Slip vectors

The Zagros must contribute to the N–S shortening of Iran within the Arabia–Eurasia collision zone. The way in which it does this is revealed by the slip vectors of the earthquakes. Each focal mechanism has two potential slip vectors (the normals to the two nodal planes) and, in general, we don't know which one was the actual slip vector, as we don't know which nodal plane was the fault plane. We therefore proceeded as follows. For strike-slip events on or near the known strike-slip systems of the Main Recent Fault and the central Zagros (51–53°E), we assumed the nodal plane subparallel to the known fault was the fault plane, which was right-lateral in each case. Most of the reverse and thrust faulting solutions have rakes close to pure dip-slip and both slip vectors have very similar azimuths. In these cases we chose the north-dipping nodal plane as the fault plane if the dip was less than 60°. In only a few cases (∼10 per cent of the total), such as strike-slip events that were not near known faults or strongly oblique thrusts, we had no good reason to chose a slip vector, and these events we ignored. The resulting horizontal projections of the slip vectors are shown in Fig 8, where we separate the strike-slip from the thrust events. In each case we show the motion of the south or west side relative to the north or east.

Fig. 8 shows some clear patterns. In general, the slip vectors on the thrusts are nearly normal to the local trends of the anticline axes (Fig. 8a), following the change in strike of the belt east of 51°E and around the Dezful embayment. There is some variation from this pattern, particularly from the poorer quality focal mechanisms (white arrows) and also around the complicated region of the syntaxis associated with the Oman Line (56–57°E; Fig. 7), where intra-continental shortening in the Zagros changes in the east to subduction beneath the Makran (Kadinsky-Cade & Barazangi 1982; Jackson & McKenzie 1984; Maggi *et al.* 2000a).

Slip vectors on strike-slip faults (Fig. 8b) are subparallel to the Main Recent Fault and the regional strike in the northern Zagros, where they are also roughly perpendicular to those of the thrusts (Fig. 8a). This confirms earlier suggestions that in this part of the Zagros the shortening and strike-slip components of the overall oblique N–S convergence are spatially separated ('partitioned'). East of 53°E there are almost no strike-slip solutions, and the slip vectors on the thrusts are subparallel to overall N–S Arabia–Eurasia motion, suggesting that no partitioning occurs, and that all the convergence is achieved by shortening on thrusts (or folds, at the surface). The region between 51°E and 53°E marks a change between a partitioned fault configuration to the NW and a non-partitioned configuration to the SE. This region contains a set of a least four roughly N–S right-lateral strike-slip faults, with slip vectors that are quite variable, but in general subparallel to either the regional strike (NW–SE) or to the N–S overall convergence. The strike-slip faults in this region must somehow accommodate the change from a partitioned to non-partitioned fault configuration. We discuss how it does so in Section 5.1.

4.3 Centroid depths

Fig. 9 displays the centroid depths determined from body wave modelling. These vary from about 4 to 20 km, with typical uncertainties being ±4 km. This nonetheless represents a much more restricted range than is evident in either the Harvard CMT catalogue or the relocated catalogue of Engdahl *et al.* (1998), as Fig. 10 and Maggi *et al.* (2000a) demonstrate. All the seismicity appears to be confined to the upper half of the crust, which is a result also found by microearthquake surveys (see references in Jackson & McKenzie 1984). The centroid depths in Fig. 9 are compatible with the majority of earthquakes occurring in the basement beneath the sedimentary cover. The thickness of this cover can be roughly estimated from the gradient of the magnetic field, and varies between about 5 km and 10 km (Morris 1977). A detailed comparison between the depth to basement calculated from aeromagnetic data and the earthquake depths will be the subject of a separate report. Some of the deepest centroids are in the Dezful embayment, where the sediment thickness is known to increase across the mountain front (see Section 4.1 and Fig. 5, inset). Within the Zagros there is, in general, no indication that the centroid depths increase northeastwards towards the Zagros Thrust Line, as might be expected if Arabia is underthrusting Iran. Only in the Oman Line syntaxis is such a pattern seen, where there is a steady northward increase in earthquake depths from about 10 km at 27.5°N to about 28 km at 28.5°N, nearly 50 km north of the Main Zagros Thrust (Fig. 7, insets a and b). Furthermore, the northernmost and deepest events have shallow north-dipping nodal planes, consistent with underthrusting of Arabian basement beneath central Iran in this particular region, confirming earlier suggestions by Kadinsky-Cade & Barazangi (1982) and Snyder & Barazangi (1986).

4.4 Reverse fault dips

We discuss the fault dips for three reasons. First, Jackson (1980b) pointed out that high-angle reverse faults (dips >30°) appeared to be more common than low-angle thrusts (dips <30°) in the Zagros. He concluded this from first-motion fault plane solutions, plotting histograms showing the dips of all nodal planes (since he was unable to chose which was the actual fault plane). He found a peak in the distribution in the range 30–60° and very few nodal plane dips corresponding to low-angle thrusts, which would plot in the ranges 0–30° and 60–90°. Fig. 11 shows histograms plotted in the same way, with the much more abundant (and higher quality) data now available. The same conclusion roughly applies, though there clearly are some solutions corresponding to low-angle thrusts, as the example in Fig. 3 demonstrates. The dominant dip range of 30–65° is indeed similar to that found for normal faults worldwide (Jackson & White 1989), which led to the suggestion that inherited normal faults beneath the stretched Arabian margin were the source of today's reverse faulting earthquakes. Whether or not this suggestion is correct, the preponderance of relatively steep (30–60°) reverse faulting in the Zagros (Fig. 11d) rules out the possibility that the earthquakes occur on a seismically active low-angle thrust or decollement underlying the whole range, as is the case in the frontal Himalaya (e.g. Ni & Barazangi 1986). If such a horizon exists beneath the Zagros, it is active aseismically and below the seismogenic layer, as it would otherwise be truncated by the active

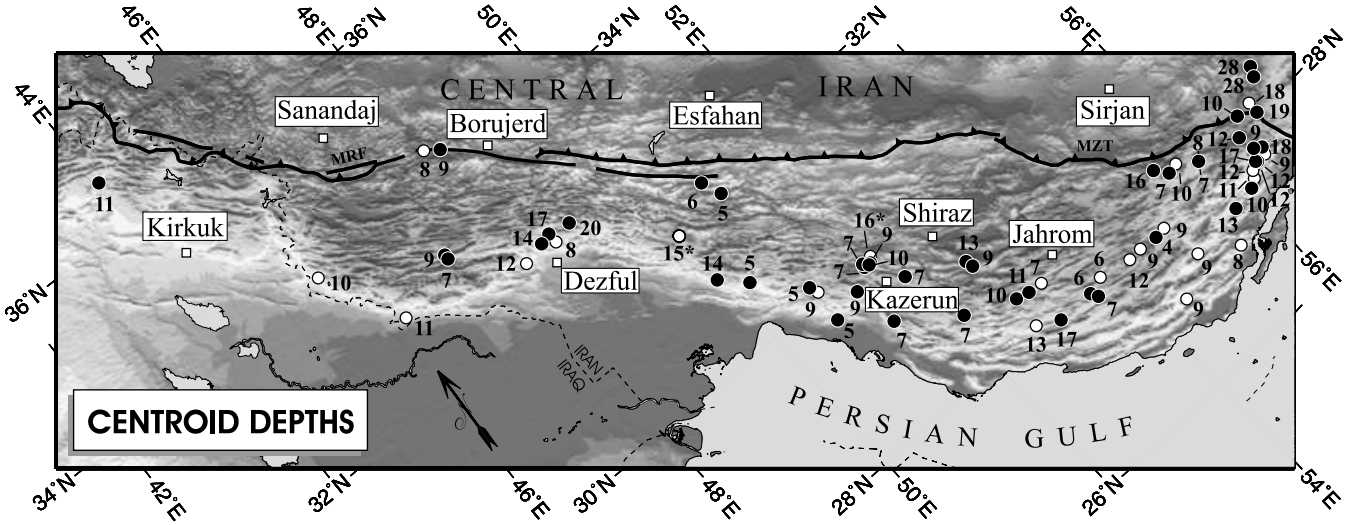

Figure 9. Earthquake centroid depths determined from waveform modelling. Numbers are depths in km. Black circles are those determined from long-period *P* and *SH* waves. Open circles are those determined from *P* waves alone. The two depths marked with stars (15* and 16*) are earthquakes whose depths were estimated from SH waves alone (Maggi *et al.* 2000a).

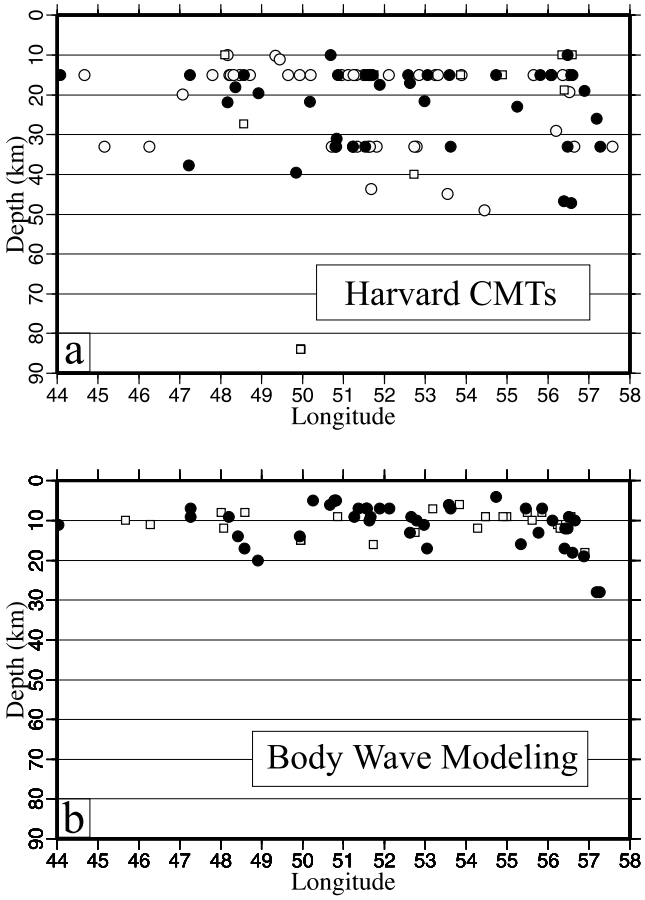

Figure 10. A comparison of centroid depths in the Zagros reported by the Harvard CMT catalogue (a) with those determined from waveform modelling (b). Black circles are those earthquakes that have both a CMT depth and a depth determined from *P* and *SH* waveforms. Open circles are those in the CMT catalogue that we could not investigate independently. Open squares are those whose depths were independently determined from *P* waves alone. The concentration of CMT depths at 15 km and 33 km are because depths are sometimes fixed to those values in the CMT solutions. The CMT depth at 84 km is the event on 1985 March 27 investigated by Maggi *et al.* (2000a), who concluded it was instead at 10–15 km depth. Note that the well-determined depths in (b) are restricted to less than 20 km, except for two earthquakes at 28 km that are at the northern end of the Oman Line (Fig. 7, inset b), and are not really in the Zagros.

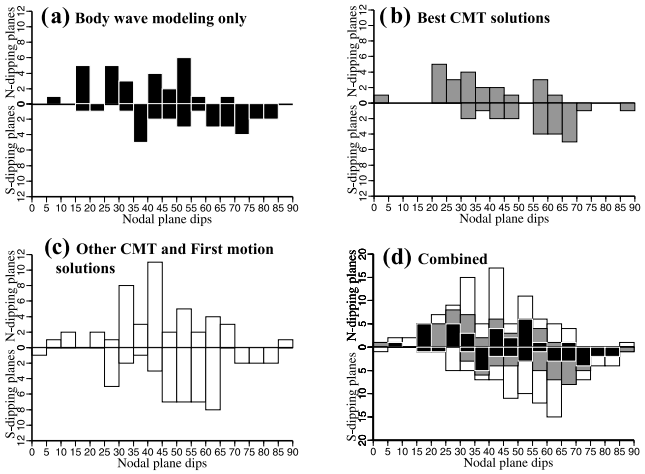

Figure 11. Histograms of nodal plane dips for reverse and thrust faulting earthquakes (with rake in the range 60–120°). Both nodal planes are included for each earthquake. (a) Earthquakes whose mechanisms are determined by *P* and *SH* body wave modelling, and N- or NE-dipping planes are distinguished from those dipping S or SW. (b) The 'best' CMT solutions, with $M_w \geq 5.3$ and >70 per cent double-couple component. (c) Other CMT solutions. (d) All earthquakes in (a)–(c) combined.

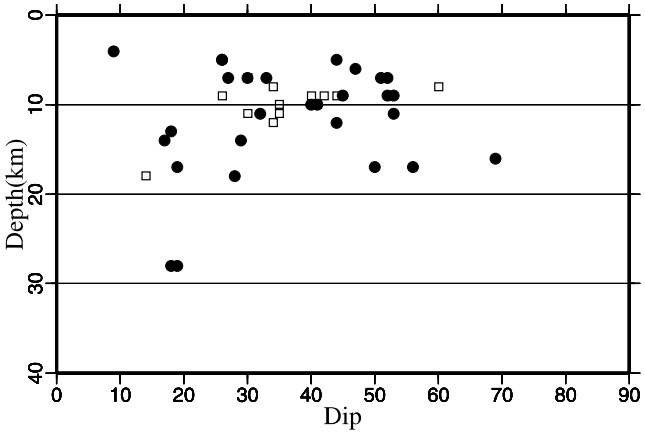

Figure 12. A plot of the dips of north-dipping nodal planes for reverse and thrust earthquakes against their centroid depths. Black circles are events constrained by *P* and *SH* modelling. Open circles are those constrained by *P* waveforms alone. The aim of this plot was to see whether the deeper events had shallower dips, as might be expected if the steeper nodal planes were faults splaying off deeper, flatter thrusts. Except near the northern end of the Oman Line (Fig. 7), where both the earthquakes at 28 km occurred, there is no convincing correlation.

reverse faults. Only in the northern part of the Oman Line syntaxis is there evidence for such a low-angle, seismically active thrust fault of regional extent (Section 4.3 and Fig. 7).

Secondly, we would like to know whether the major thrusts dip N–NE or S–SW. In Fig. 11, the N- and NE-dipping nodal planes are distinguished (top) from the S- and SW-dipping planes (bottom). In general, the histograms are asymmetric, with the N-dipping planes biased towards shallower dips of typically 30–45°, and the S-dipping planes being somewhat steeper, in the range 45–60°. This is indeed what we would expect if the shallower-dipping nodal planes are the rupture planes and if the thrusts generally dip N or NE, as is suggested by the asymmetry of the folds at the surface. But since we have no independent confirmation of which nodal plane is in fact the rupture plane, this evidence is suggestive, not conclusive.

Thirdly, given the presence of at least some low-angle thrusts and also the dominant asymmetry of the Zagros folds, with the steepest limb on the SW side, we checked whether there was any correlation between the dip of the north-dipping nodal plane (likely to be the fault plane) and the centroid depth (Fig. 12). If the steeper reverse faults were splaying off more gently dipping thrusts at depth, we might expect such a correlation, as is indeed seen, for example, in the Hellenic subduction zone south of Crete (Taymaz *et al.* 1990). Such a pattern is perhaps seen at the northern part of the Oman Line syntaxis (Section 4.3, Fig. 7). But no convincing correlation exists in the main part of the Zagros, where some of the lowest dips correspond to the shallowest earthquakes (e.g. Fig. 3).

5 DISCUSSION

5.1 The role of strike-slip faulting in the collision

A major tectonic question is how the configuration of active faulting in the Zagros contributes to the N–S shortening of the Arabia–Eurasia collision. The earthquake slip vectors in Fig. 8 show that the principal characteristic of the Zagros is that in the NW the oblique convergence is partitioned into its orthogonal strike-slip and shortening components, whereas in the SE, where the convergence is perpendicular to the thrust belt, there is no partitioning or strike-slip faulting. The change from partitioning to no partitioning along strike of the belt requires the region in the NW, between the Main Recent Fault and the SW border of the Zagros, to be moving NW

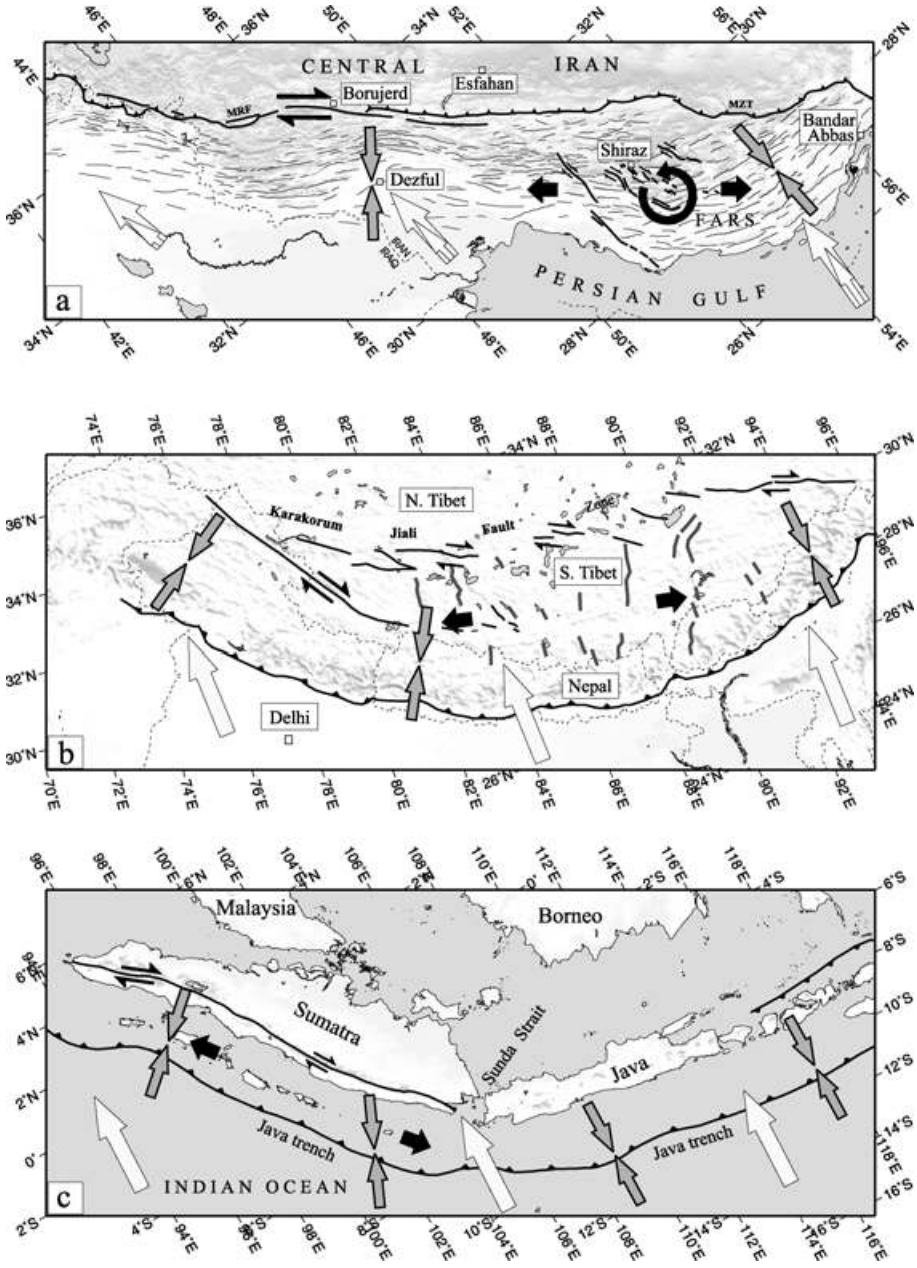

Figure 13. (a) Summary sketch of the tectonic pattern in the Zagros. Overall Arabia–Eurasia motions are shown by the big white arrows, as before. In the NW Zagros (Borujerd-Dezful), oblique shortening is partitioned into right-lateral strike-slip on the Main Recent Fault (MRF) and orthogonal shortening (large gray arrows). In the SE Zagros (Bandar Abbas) no strike-slip is necessary, as the shortening is parallel to the overall convergence. The central Zagros (Shiraz) is where the transition between these two regimes occurs, with anticlockwise rotating strike-slip faults allowing an along-strike extension (black arrows) between Bandar Abbas and Dezful. (b) A similar sketch for the Himalaya (after McCaffrey & Nábělek 1998). In this case the overall Tibet-India motion is likely to be slightly west of north. (The India-Eurasia motion is about 020°, but Tibet moves east relative to both India and Eurasia: Wang *et al.* 2001). Thrust faulting slip vectors are radially outward around the entire arc (gray arrows). This leads to partitioning of the oblique convergence in the west, where right-lateral strike-slip is prominent on the Karakoram Fault, but no strike-slip in the east, where the convergence and shortening are parallel. The region in between extends parallel to the arc, on normal faults in southern Tibet. (c) A similar sketch for the Java–Sumatra arc, based on McCaffrey (1991). Slip partitioning occurs in the NW, with strike-slip faulting through Sumatra, but not in the SE, near Java. This change along the zone requires the Java–Sumatra forearc to extend along strike.

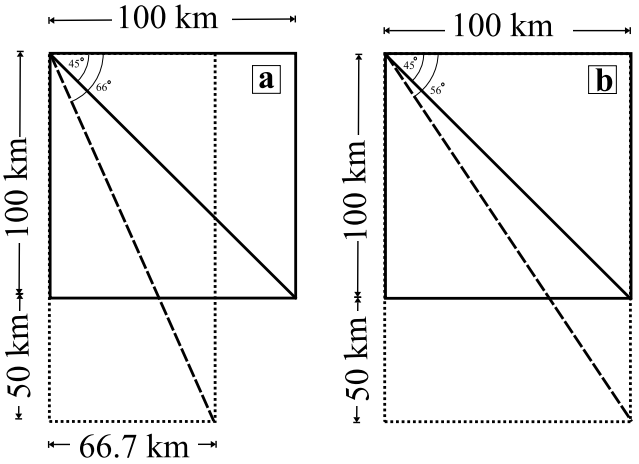

Figure 14. Simplistic cartoons to illustrate possible relations between fault rotations and shortening in the central Zagros (see text). (a) Surface area is preserved, with faults originally at 66° to the zone rotating to an angle of 45°. (b) Surface area is not preserved, and no along-strike extension occurs. In this case faults rotate only from 56° to 45 °. In both (a) and (b) the faults are assumed to be passive markers, and the blocks they bound are not internally rigid.

(i.e. along strike) relative to the Fars region in the SE part of the belt (east of 53°E). This in turn requires an extension along strike of the belt, which can be achieved by the right-lateral strike-slip fault systems between 51°E and 53°E if they rotate anticlockwise about vertical axes (Fig. 13a). Thus the function of the zone of strike-slip faulting in the central Zagros is to accommodate the fundamental change in shortening modes to either side. The essential characteristic of these strike-slip faults is that they appear to end in thrusts that die away with distance from their junction with the strike-slip faults. This is seen clearly in the geological and seismological evidence at the southern termination of the Karebas Fault (Fig. 6, SW inset, and Section 4.1) and also in the geomorphology and geology at both ends of the Sarvestan Fault (Fig. 6, see Berberian 1995 for geological details). These characteristics are typical of intra-continental strike-slip fault terminations and allow them to fulfil the role of permitting a change in the mode of shortening along the strike of a mountain belt (Bayasgalan *et al.* 1999).

In this case, we can make some estimate of the amount of rotation that is required if the faults rotate as passive markers in a distributed deformation field. If we assume that the current shortening rate across the Zagros of ∼10 mm yr^{-1} has operated for 5 Ma (roughly in agreement with the available GPS and stratigraphic estimates), then the total shortening across the Simple Folded Belt should be no more than about 50 km. This estimate is similar to that obtained from structural estimates across the whole Zagros (e.g. Falcon 1974). The central Zagros strike-slip system currently occupies about a 100 km width of the Simple Folded Belt, which was therefore up to ∼150 km wide prior to shortening. The strike-slip faults are currently ∼45° to the strike of the belt. An upper bound to the rotation is obtained if we assume surface area is preserved (which it obviously is not), giving maximum along-strike extension (∼33 km), in which case the faults were previously at a higher angle to the belt of about 66° (Fig. 14a). A lower bound is obtained if we assume no along-strike extension, in which case the original angle to the belt was only about 56° (Fig. 14b). Thus, in this simple model of distributed deformation, the expected amount of clockwise rotation may be as much as 10–20° (if the shortening is as much as 50 km), and possibly measurable by paleomagnetism, if suitable rocks are available. The amount of along-strike extension in Fig. 14(a) is also similar (given the extreme simplicity of the above calculations) to the offset of ∼50 km on the Main Recent Fault (Talebian & Jackson 2002), which it should be. However, the fault-bounded blocks may rotate rigidly or semi-rigidly, rather than in the distributed continuous manner described above. A more thorough examination of the relations between faulting and rotations in this region requires detailed analysis of the geology and offsets on the faults, which will be reported elsewhere.

In reality, the region between the Main Recent Fault and the SW border of the Zagros is not a rigid unit, and some variations along strike are also seen at a smaller scale. Thus on the northern edge of the Dezful embayment (Fig. 5, inset), where the mountain front trends E–W, slip vectors on the thrusts and reverse faults are again similar to the direction of overall N–S convergence (Fig. 8a), and less oblique to that direction than they are to the NW or SE. This reduces, locally, the need for partitioning, and effects like this may lead to variations in total strike-slip offset along the Main Recent Fault.

Other studies have also suggested that rotation of the strike-slip faulting in the central Zagros is an important element in the collision tectonics. Hessami *et al.* (2001a) suggest a similar scheme to ours in Fig. 13(a), except that they invoke conjugate left- and right-lateral faults in the southern Zagros in a buckling configuration that is an adaptation of a model presented for the northern Aegean Sea by Taymaz *et al.* (1991). Our principal objection to their scheme is that we see no seismological evidence for the NE-SW trending left-lateral faults that Hessami *et al.* (2001a) invoke east of 53°E. Their main evidence for the existence of these faults is based on apparent disturbances to anticline axes seen on satellite imagery. It is possible that, for reasons unknown, the left-lateral faults are both much less clearly expressed at the surface and much less seismically active than the right-lateral faults, but it seems to us unlikely. Furthermore, the left-lateral faults (if they exist) have no obvious role in a region where the thrust-faulting slip vectors are anyway parallel to the overall convergence. But in other essentials the model of Hessami *et al.* (2001a) is similar to ours, in particular in its requirement for along-strike extension. Hessami *et al.* (2001a) also suggest that the extensional component is responsible for the preferential localization of some Hormuz Salt plugs along the strike-slip faults. Numerous authors have pointed out that the N–S right-lateral strike-slip faults appear to be reactivations of structural trends seen in Arabia (e.g. Falcon 1974; Hessami *et al.* 2001a).

Finally, it is remarkable how similar is the kinematic scheme we are proposing for the Zagros in Fig. 13(a) to those in both the Himalaya (Fig. 13b, McCaffrey & Nábělek 1998) and in the Java–Sumatra subduction zone (Fig. 13c, McCaffrey 1991). In all three places, curvature of the belt causes a change from orthogonal to oblique convergence along strike, and the oblique shortening is achieved by partitioning. The resultant along-strike extension is achieved by strike-slip faulting in Indonesia and the Zagros, and by normal faulting in southern Tibet.

5.2 Distribution of the faulting

On geological maps, satellite images and in the field, the Zagros is a strikingly uniform mountain belt. At the surface, shortening has obviously occurred in much the same way across most of the width of the belt, though different stratigraphic levels are exposed in different places. As Berberian (1995) points out, important changes in

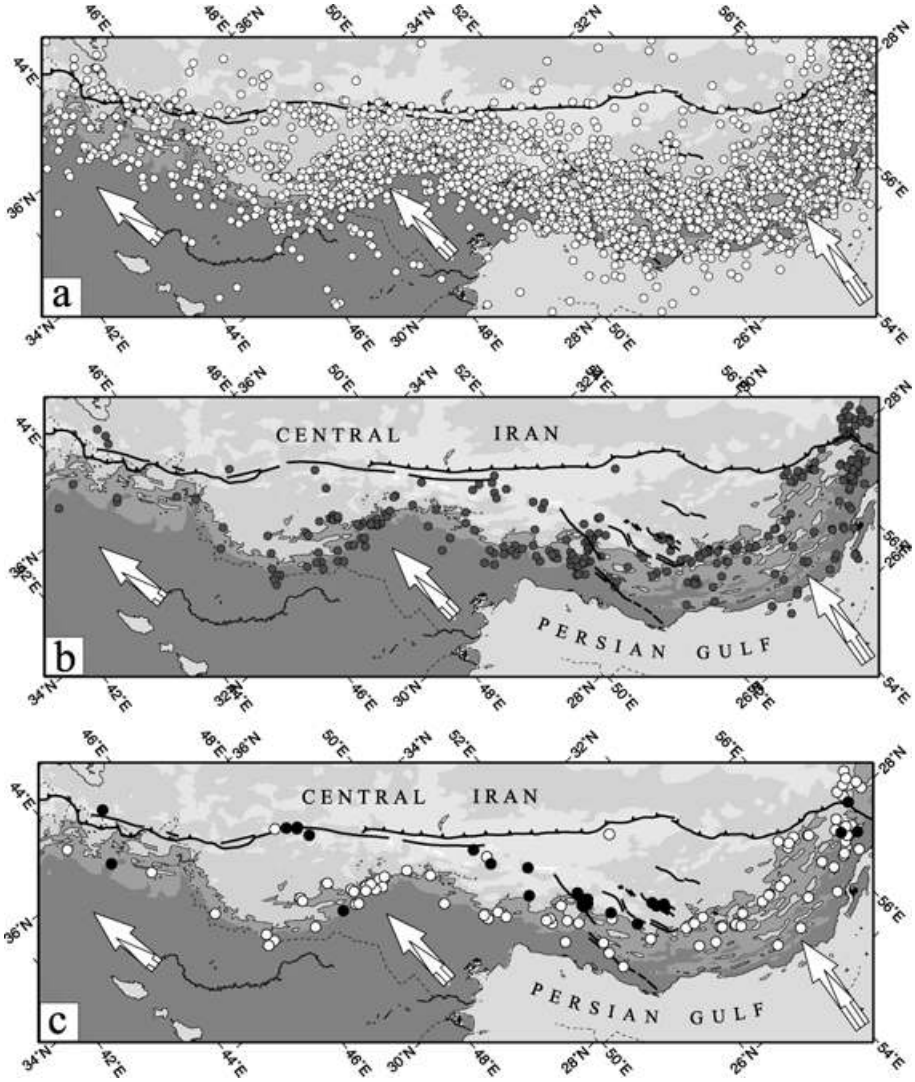

Figure 15. (a) A map showing all the earthquakes in the ISC catalogue between 1964 and 2002, with the Main Recent Fault and Main Zagros Thrust shown for location. White arrows are overall Arabia–Eurasia motions, as before. Shading of the topography changes at 500, 1000, 2000 and 3000m levels, and the 1000 m level is contoured. Note how these earthquakes are distributed over most of the width of the belt. (b) As in (a), but only the earthquakes with $m_b \geq 5.0$ are plotted, taken from the Engdahl *et al.* (1998) catalogue. (c) As in (a) but only earthquakes whose mechanisms are in Figs 5–7 are plotted, with open circles for reverse and thrusts faults and black circles for strike-slip. These are necessarily the bigger events, nearly all of them above M_w 5.3. Note how the high topography is virtually aseismic at this level, except for strike-slip faults. Most of the reverse and thrust faulting earthquakes occur at the edge of the topography, between 500 and 1000 m.

structural and stratigraphic level may indicate sites of deep basement thrusting which, if his interpretation is correct, is less evenly distributed than the folding at the surface and instead concentrated on relatively few major basement faults. Yet the most obvious feature of the seismicity is that the larger earthquakes are even more restricted, though small earthquakes occur right across the belt (Figs 1 and 15a). We therefore conclude that most of the major basement faults in the NE Zagros identified by Berberian (1995) are probably inactive today (Figs 5–7), and the highest topography of the Zagros is conspicuously devoid of the larger earthquakes, except for ones on the strike-slip faults (Figs 15b and c). The active shortening on basement faults is instead concentrated around the edge of the topography. This is no surprise, as shear stresses are expected to be greatest near gradients in crustal thickness, rather than under the highest topography itself (England & McKenzie 1982). We therefore suspect that Berberian's (1995) assertion that basement faulting is restricted to a few major structures is correct, but that the activity has shifted from one fault to another with time. Microseismicity is, however, much more distributed (e.g. Tatar 2001), and so is folding of the sedimentary cover, which is decoupled from the basement by evaporites. Today's earthquake locations thus reflect the general migration of activity towards the foreland in the SW, which can be seen in the stratigraphy as well (Falcon 1974; Berberian 1995; Hessami *et al.* 2001b) and is a common feature of fold-and-thrust belts.

5.3 Accommodation of Arabia–Iran shortening

The present-day configuration of faulting in the Zagros is able to accommodate N–S shortening between Arabia and central Iran, as part of the general N–S shortening in the Arabia–Eurasia collision zone. The essential characteristic of the shortening is relatively high-angle reverse faulting in the basement beneath folding at the surface. An

additional complication is the change along strike from partitioned oblique shortening in the NW to almost orthogonal shortening in the SE, with the junction between the two regimes being accommodated by rotating strike-slip faults in the central Zagros.

It is still unclear just how closely tied the sites of active basement faulting are to those of active surface folding, and the extent to which the two are spatially separated by decoupling horizons within the sediments. This issue will need other observations, such as GPS or InSAR measurements. Nonetheless, the similarity of the structures across the width of the Simple Folded Belt, and the probability of relatively few discrete basement faults as well, suggests that it is the location, rather than the style, of shortening in the Simple Folded Belt that has changed over the last 5 Ma. Thus the upper part of the stretched Mesozoic margin of Arabia has probably shortened by distributed reverse faulting and folding. If a regional low-angle thrust surface exists it is evidently not active seismically and presumably creeps at depths beneath the seismogenic layer (see e.g. Snyder & Barazangi 1986). In this respect the Zagros is clearly different from the Himalaya, where low-angle thrusting is active seismically throughout the region beneath the lesser Himalaya to a depth of at least 15 km (e.g. Ni & Barazangi 1986). In the case of the Himalaya, there is evidence in both the earthquake locations and the seismic anisotropy that the Indian shield underthrusts southern Tibet to a distance of at least 300 km beyond the Indus-Tsangpo suture (the northern limit of the Indian margin at the surface) and to a depth of ∼80 km (Huang *et al.* 2000; Jackson 2002). By contrast, within the main part of the Zagros there is no such evidence in the earthquakes that the basement of Arabia underthrusts central Iran to any significant degree. Perhaps this is not surprising: the amount of convergence since the suturing between India and southern Tibet ∼50 Ma ago is much greater (perhaps 1000 km) than that between Arabia and central Iran since they finally sutured 5–10 Ma ago (perhaps 50–100 km). Furthermore, the Indian shield is known to be unusually strong, with an effective elastic thickness of ∼40 km (McKenzie & Fairhead 1997; Jackson 2002), perhaps predisposing it to rigid underthrusting of Tibet, whereas the Arabian shield beneath the Persian Gulf has an effective elastic thickness of only ∼15 km and is significantly weaker (Maggi *et al.* 2000b). The only site where there is plausible seismic evidence for the underthrusting of the Arabian basement beneath the Zagros-central Iran suture is at the SE end of the belt, near the syntaxis of the Oman Line (Fig. 7, Section 4.3 and 4.4). In this region (near 57°E) low-angle north-dipping thrusting earthquakes occur for about 50 km north of the suture, with centroid depths increasing northwards to a depth of nearly 30 km. Given the complications of the syntaxis, this interpretation is obviously ambiguous, though it could potentially be checked with a profile of seismic receiver functions.

6 CONCLUSIONS

The Simple Folded Belt of the Zagros resembles a carpet, folding (and to some extent faulting) above a basement that is fractured by large faults. The carpet obscures our view of the basement, and since coseismic surface faulting is so rare, earthquakes provide the most abundant and accessible information about the active faulting at depth. This study demonstrates, as have others in this region before (e.g. Maggi *et al.* 2000a; Jackson *et al.* 2002), that simple patterns can be seen in the earthquake data, provided proper attention is given to the data quality. In particular, patterns of fault configurations and earthquake depths may well not be evident in routinely reported catalogue data, either of hypocentres or CMT solutions. The patterns we describe in the Zagros are not new, in the sense that they reveal processes that are also known in other mountain belts. But they are hidden or obscured by bad data, and it is important to extract those patterns if we are to consider the reasons for the different structural behaviour of mountain belts. Such contrasts between belts are likely to become increasingly important. For example, the Zagros shows some similarities with the Himalaya, such as the consequences of along-strike curvature of the belt, but also profound differences, such as the lack of seismic or other evidence for low-angle underthrusting of the frontal part of the range. These structural contrasts may well reflect the influence of fundamental properties, such as the strength of the bounding forelands (e.g. Maggi *et al.* 2000b; Jackson 2002), and it is therefore important to articulate them if we are to make progress in understanding the controls on continental dynamics.

ACKNOWLEDGMENTS

We thank K. Priestley for help with waveform preparation, M. Allen and M. Berberian for numerous discussions of Zagros tectonics, and D. Hatzfeld for a constructive review. We particularly thank M. Korehie and M. Ghorashi of the Geological Survey of Iran for their constant support of our research in Iran over many years. MT thanks Amerada Hess, King's College, the Cambridge Overseas Trust and the Foreign & Commonwealth Office for scholarships enabling him to study in Cambridge supported by NERC Centre for the Observation and Modelling of Earthquakes and Tectonics (COMET). Cambridge Earth Sciences contribution ES 7509.

REFERENCES

Ambraseys, N.N., 1978. The relocation of the epicentres in Iran, *Geophys. J. R. astr. Soc.*, **53,** 117–121.

Badley, M.E., Price, J.D. & Backshall, L.C., 1989. Inversion, reactivated faults and related structures: seismic examples from North sea, in, *Inversion Tectonics*, Vol. 44, pp. 201–219, eds Cooper, M.A., & Williams, G.D., Geol. Soc. Spec. Publ. London.

Baker, C., 1993. The active seismicity and tectonics of Iran, *PhD. thesis*, University of Cambridge, UK, p. 228.

Baker, C., Jackson, J. & Priestley, K., 1993. Earthquakes on the Kazerun Line in the Zagros Mountains of Iran: strike-slip faulting within a fold-and-thrust belt, *Geophys. J. Int.*, **115,** 41–61.

Bayasgalan, A., Jackson, J., Ritz, J.F. & Cartier, S., 1999. Field examples of strike-slip fault terminations in Mongolia and their tectonic significance, *Tectonics*, **18,** 394–411.

Berberian, M., 1979. Evaluation of the instrumental and relocated epicentres of Iranian earthquakes, *Geophys. J. R. astr. Soc.*, **58,** 625–630.

Berberian, M., 1995. Master blind thrust faults hidden under the Zagros folds: active basement tectonics and surface morphotectonics, *Tectonophysics*, **241,** 193–224.

Berberian, M. & King, G., 1981. Towards a paleogeography and tectonic evolution of Iran, *Can. J. Earth Sci.*, **18,** 210–265.

Bird, P., Toksoz, M. & Sleep, N., 1975. Thermal and mechanical models of continent-continent convergence zones, *J. geophys. Res.*, **80,** 4405–4416.

Chu, D. & Gordon, R.G., 1998. Current plate motions across the Red Sea, *Geophys. J. Int.*, **135,** 313–328.

Devlin, W.J., Cogswell, J.M., Gaskins, G.M., Isaksen, G.H., Pitcher, D.M., Puls, D.P., Stanley, K.O. & Wall, G.R.T., 1999. South Caspian basin: young, cool, and full of promise, *GSA Today*, **9,** 1–9.

De Mets, C., Gordon, R.G., Argus, D.F. & Stein, S., 1994. Effects of recent revision to the geomagnetic reversal time scale on estimates of current plate motions, *Geophys. Res. Lett.*, **21,** 2191–2194.

Dziewonski, A.M., Chou, T.A. & Woodhouse, J.H., 1981. Determination of earthquake source parameters from waveform data for studies of global and regional seismicity, *J. geophys. Res.*, **86,** 2825–2852.

Engdahl, E.R., van der Hilst, R. & Buland, R., 1998. Global teleseismic earthquake relocation with improved travel times and procedures for depth determination, *Bull. seism. Soc. Am.*, **88,** 722–743.

England, P.C. & McKenzie, D., 1982. A thin viscous sheet model for continental deformation, *Geophys. J. R. astr. Soc.*, **70,** 295–321.

Falcon, N.L., 1974. Southern Iran: Zagros Mountains, in, *Mesozoic-Cenozoic Orogenic Belts, Data for Orogenic Studies,* Vol. 4, pp. 199–211, ed. Spencer, A.M., Geol. Soc. Spec. Publ. London.

Harvard University, Department of Geological Sciences, 2000. Centroid Moment Tensor catalogue, available online at: http://www.seismology.harvard.edu/CMTsearch.html.

Haynes, S.J. & McQuillan, H., 1974. Evolution of the Zagros suture zone, southern Iran, *Geol. Soc. Am. Bull.*, **85,** 739–744.

Hessami, K., Koyi, H.A. & Talbot, C.J., 2001a. The significance of strike-slip faulting in the basement of the Zagros fold and thrust belt, *J. Petrol. Geol.*, **24,** 5–28.

Hessami, K., Koyi, H.A., Talbot, C.J., Tabasi, H. & Shabanian, E., 2001b. Progressive unconformities within an evolving foreland fold-thrust belt, Zagros Mountains, *J. geol. Soc. Lond*, **158,** 969–981.

Hessami, K., 2002. Tectonic history and present-day deformation in the Zagros fold-thrust belt, *PhD thesis*, University of Uppsala, Sweden.

Huang, W.C. *et al.*, 2000. Seismic polarization anisotropy beneath the central Tibetan Plateau, *J. geophys. Res.*, **105,** 27 979–27 989.

Jackson, J.A., 1980a. Errors in focal depth determination and the depth of seismicity in Iran and Turkey, *Geophys. J. R. astr. Soc.*, **61,** 285–301.

Jackson, J.A., 1980b. Reactivation of basement faults and crustal shortening in orogenic belts, *Nature*, **283,** 343–346.

Jackson, J.A., 2002. Strength of the continental lithosphere: Time to abandon the jelly sandwich?, *GSA Today*, **12,** 4–10.

Jackson, J.A. & Fitch, T.J., 1981. Basement faulting and the focal depth of the larger earthquakes in the Zagros mountains (Iran), *Geophys. J. R. astr. Soc.*, **64,** 561–586.

Jackson, J. & McKenzie, D., 1984. Active tectonics of the Alpine-Himalayan belt between western Turkey and Pakistan, *Geophys. J. R. astr. Soc.*, **77,** 185–264.

Jackson, J.A. & McKenzie, D., 1988. The relationship between plate motions and seismic moment tensors, and the rates of active deformation in the Mediterranean and Middle East, *Geophys. J.*, **93,** 45–73.

Jackson, J.A. & White, N.J., 1989. Normal faulting in the upper continental crust: observation from regions of active extension, *J. Struct. Geol.*, **11,** 15–36.

Jackson, J.A., Haines, A.J. & Holt, W.E., 1995. The accommodation of the Arabia–Eurasia plate convergence in Iran, *J. geophys. Res.*, **100,** 15 205–15 219.

Jackson, J., Priestley, K., Allen, M.B. & Berberian, M., 2002. Active tectonics of the South Caspian Basin, *Geophys. J. Int.*, **8, 148,** 214–245.

Jestin, F., Huchon, P. & Gaulier, J.M., 1994. The Somalia plate and the East African rift system: present-day kinematics, *Geophys. J. Int.*, **116,** 637–654.

Kadinsky-Cade, K. & Barazangi, M., 1982. Seismotectonics of southern Iran: the Oman Line, *Tectonics*, **1,** 389–412.

Koop, W.J. & Stoneley, R., 1982. Subsidence history of the Middle East Zagros basin, Permian to Recent, *Phil. Trans. R. Soc. Lond.*A., **305,** 149–168.

Maggi, A., Jackson, J.A., Priestley, K. & Baker, C., 2000a. A re-assessment of focal depth distributions in southern Iran, the Tien Shan and northern India: do earthquakes really occur in the continental mantle?, *Geophys. J. Int.*, **143,** 629–661.

Maggi, A., Jackson, J.A., McKenzie, D. & Priestley, K., 2000b. Earthquake focal depths, effective elastic thickness, and the strength of the continental lithosphere, *Geology*, **28,** 495–498.

McCaffrey, R., 1991. Slip vectors and stretching of the Sumatran fore arc, *Geology*, **19,** 881–884.

McCaffrey, R. & Abers, G., 1988. SYN3: a program for inversion of teleseismic body waveforms on microcomputers, *Air Force Geophysics Laboratory Technical report, AFGL-TR-88-0099*, Hanscomb Air Force Base, Massachusetts.

McCaffrey, R. & Nábělek, J., 1987. Earthquakes, gravity and the origin of the Bali basin: an example of a nascent continental fold-and-thrust belt, *J. geophys. Res.*, **92,** 441–460.

McCaffrey, R. & Nábělek, J., 1998. Role of oblique convergence in the active deformation of the Himalayas and southern Tibet plateau, *Geology*, **26,** 691–694.

McCaffrey, R., Zwick, P. & Abers, G., 1991. SYN4 Program, IASPEI software Library, **3,** 81–166.

McCall, G.J.H., 1996. The inner Mesozoic to Eocene ocean of south and central Iran and associated microcontinents, *Geotectonics*, **29,** 490–499.

McKenzie, D.P., 1972. Active tectonics of the Mediterranean region, *Geophys. J. R. astr. Soc.*, **30,** 109–185.

McKenzie, D.P. & Fairhead, D., 1997. Estimates of the effective elastic thickness of the continental lithosphere from Bouguer and free air gravity anomalies, *J. geophys. Res.*, **102,** 27 523–27 552.

Molnar, P. & Lyon-Caen, H., 1989. Fault plane solutions of earthquakes and active tectonics of the Tibetan Plateau and its margin, *Geophys. J. Int.*, **99,** 123–153.

Moores, E.M. & Twiss, R.J., 1995. *Tectonics*, W.H. Freeman, New York.

Morris, P., 1977. Basement structure as suggested by aeromagnetic survey in S.W. Iran, Oil Service Company of Iran, internal report.

Nábělek, J., 1984. Determination of earthquake source parameters from inversion of body waves, *PhD thesis*, Massachusetts Institute of Technology.

Ni, J. & Barazangi, M., 1986. Seismotectonic of the Zagros Continental Collision Zone and a Comparison With the Himalayas, *J. geophys. Res.*, **91,** 8205–8218.

North, R.G., 1974. Seismic slip rates in the Mediterranean and Middle East, *Nature*, **252,** 560–563.

Nowroozi, A., 1971. Seismotectonics of the Persian Plateau, Eastern Turkey, Caucasus, and Hindu Kush Region, *Bull. seism. Soc. Am.*, **61,** 317–341.

Raisi, M., 1991. The Darab, Iran Earthquake of 6 Nov. 1990, *BSc. thesis*, University of Shiraz, Iran.

Ricou, L.E., Braud, J. & Brunn, J.H., 1977. Le Zagros, *Mem. h. ser. Soc. geol. France*, **8,** 33–52.

Sella, G.F., Dixon, T.H. & Mao A., 2002. REVEL: A model for Recent plate velocities from space geodesy, *J. geophys. Res.*, **107,** 10.1029/2000JB000033.

Setudehnia, A., 1978. The Mesozoic sequence in south-west Iran and adjacent area, *J. Petrol. Geol.*, **1,** 3–42.

Scholz, C.H., 1982. Scaling laws for large earthquakes: consequences for physical models, *Bull. seism. Soc. Am.*, **72,** 1–14.

Sharland, R.R., Archer, R., Casey, D.M., Davies, R.B., Hall, S.H., Heward, A.P., Horbury A.D. & Simmons, M.D., 2001. *Arabian plate sequence stratigraphy*, GeoArabia, Special Publication 2, GulfPetroLink, Bahrain, p. 371.

Shirakova, E.I., 1967. General features in the orientation of principal stresses in earthquake foci in the Mediterranean-Asian seismic belt, *Earth Physics,* **1,** 22–36.

Snyder, D.B. & Barazangi, M., 1986. Deep crustal structure and flexure of the Arabian plate beneath the Zagros from Gravity observations, *Tectonics*, **5,** 361–373.

Stöcklin, J., 1974. Possible ancient continental margins in Iran, in *The Geology of Continental Margins*, pp. 873–887, eds Burke, C.A. & Drake, C.L., Springer-Verlag, New York.

Stoneley, R., 1976. On the origin of ophiolite complexes in the southern Tethys region, *Tectonophysics*, **25,** 303–322.

Stoneley, R., 1981. The geology of the Kuh-e-Dalneshin area of southern Iran, and its bearing on the evolution of southern Tethys, *J. Geol. Soc. London*, **138,** 509–526.

Talbot, C.J., 1998. Extrusion of Hormuz salt in Iran, *Geol. Soc. Spec. Publ. London*, **143,** 315–334.

Talebian, M. & Jackson, J.A., 2002. Offset on the Main Recent Fault of NW Iran and implication for the late Cenozoic tectonics of the Arabia–Eurasia collision zone, *Geophys. J. Int.*, **150,** 422–439.

Tatar, M., 2001. Etude Sismotectonique de deux zones de collision continentale: le Zagros Central et l'Alborz (Iran)., *PhD thesis*, University of Joseph Fourier, Grenoble I, France, p. 204.

Tatar, M., Hatzfeld, D., Martinod, J., Walpersdorf, A., Ghafori-Ashtiany, M. & Chery, J., 2002. The present-day deformation of the central Zagros from GPS measurements, *Geophys. Res. Lett.*, **29,** 1927, doi:10.1029/2002/GL015427.

Taymaz, T., Jackson, J.A. & Westaway, R., 1990. Earthquake mechanisms in the Hellenic trench near Crete, *Geophys. J. Int.*, **102,** 695–731.

Taymaz, T., Jackson, J.A. & McKenzie, D., 1991. Active tectonics of the north and central Aegean Sea, *Geophys. J. Int.*, **106,** 433–490.

Tchalenko, J.S. & Braud, J., 1974. Seismicity and structure of the Zagros: the Main Recent Fault between 33° and 35°N, *Phil. Trans. R. Soc. Lond.*A., **277,** 1–25.

United States Geological Survey, Earthquake Hazards Program, National Earthquake Information Centre, World Data Center for Seismology, Denver, 2002. Earthquake Data Base, available on line at: http://neic.usgs.gov/neis/epic/epic.html.

Walker, R., 2003. Active faulting and tectonics of eastern Iran, *PhD thesis,* University of Cambridge, 204pp.

Wang, Q. *et al.,* 2001. Present-Day crustal Deformation in China Constrained by Global Positioning System Measurements, *Science*, **294,** 574–577.

Zwick, P., McCaffrey, R. & Abers, G., 1994. MT5 Program, *IASPEI Software Library*, **4**.